analytical chemistry

Review

Cite This: *Anal. Chem.* 2018, 90, 65−85

pubs.acs.org/ac

Cellular Analysis Using Microfluidics

Jay Sibbitts,[†] Kathleen A. Sellens,[†] Shu Jia,[†] Scott A. Klasner,[‡] and Christopher T. Culbertson*[,†]

[†]Department of Chemistry, Kansas State University, Manhattan, Kansas 66506, United States

[‡]12966 South State Highway 94, Marthasville, Missouri 63357, United States

CONTENTS

Cells are the fundamental building blocks of life. Changes within a cell can propagate throughout much larger, more complex systems. The knowledge of how these changes arise internally within a cell and how cellular signals are transmitted through larger systems of cells, whether those systems be an organ, organism, or a larger environmental assemblage, is critical, for example, to understanding how diseases arise and spread and how cells communicate and coordinate their actions. Microfluidic devices provide unique platforms from which to study many of these intra- and intercellular processes. The architectures enabled by microfluidic fabrication methods are on length and volume scales suitable for the sorting, transport, capture, culturing, and analysis of single cells and small assemblages of cells. In addition, the secretions from cultured cells or cell lysates are not significantly diluted prior to detection, so the minute quantities of species secreted or contained in the lysate can be detected and quantified. Finally, for cells cultured on microfluidic devices, specific cells in larger arrays of cells can be perturbed and their individual responses tracked. Such capabilities have led to an explosion of increasingly integrated and sophisticated microfluidic devices for cellular analysis over the past decade. These advances are quickly being turned into microfluidic systems that can mimic complex cellular systems and detect responses of these systems to various perturbations. While, in previous years, we have written comprehensive reviews of the field of microfluidics,[1,2] this year, we have chosen to write a more focused review covering cellular analyses enabled by microfluidic devices because of the rapid pace of advancement in this area. This Review follows a similar review written for this journal previously.[3]

Cellular analyses on microfluidic devices take advantage of multiple, integrated functional elements. These elements may include cell encapsulation, cell transport/sorting, cell capture, cell culturing, a method to stimulate/perturb cells, cell secretion/lysis, secreted molecule/lysate treatment, separation, and detection. While not all of these elements need to be integrated into a cellular analysis chip, they do provide a convenient way to organize this Review. Generally, papers are referenced under the functional element areas where they make the most unique contribution. Most of the advanced, multielement, integrated devices are covered in the analysis of intact or secreted cell sections of this Review; however, if a paper also reports a significant advance in a particular functional element area, then it may also be briefly discussed in that section.

The papers included in this Review were published between September 2015 and September 2017. The material was compiled using several strategies including extensive searches using Scifinder, Web of Science, PubMed, and Google Scholar. The contents of high impact journals were also scanned, including *Analytical Chemistry*, *Lab-on-a-Chip*, *Nature*, *Proceedings of the National Academy of Sciences*, *Applied Physics Letters*, *Biosensors and Bioelectronics*, *Angewandte Chemie*, *Nano Letters*, *Science*, *Biomedical Microdevices*, *RSC Advances*, *Electrophoresis*, and *Langmuir*. Several hundred papers relating to the analysis of cells using microfluidics were examined. We have attempted to identify some of the most interesting and promising papers for this Review. Without a doubt, we have missed a few excellent papers and had to eliminate others based on space constraints

Special Issue: Fundamental and Applied Reviews in Analytical Chemistry 2018

Published: November 15, 2017

DOI: 10.1021/acs.analchem.7b04519
Anal. Chem. 2018, 90, 65−85

and readability. For those papers that we have failed to include, we apologize in advance and welcome comments regarding any oversight that we have made.

FUNCTIONAL ELEMENTS

Cell Encapsulation. The encapsulation of cells in a microfluidic system is often convenient or even necessary to protect or isolate the cells during manipulation and analysis. The usefulness of the cell containing droplets is also often dependent upon being able to create uniformly sized droplets with a controllable number of cells in each droplet. In addition, as high-throughput analysis is often sought, being able to produce the droplets quickly is of paramount importance. Several new chip designs were reported to create uniformly sized droplets in a high-throughput manner. For example, a micropillar array device enabled the encapsulation of cells in sub-50 μm diameter droplets with a generation frequency of up to 3.1 MHz.[4] The throughput of this device was higher than traditional T-junction and flow focusing chip layouts and maintained a cell viability of around 70% over a two-week culture period. Since encapsulation in oil poses potential risks of cytotoxicity, encapsulating cells in hydrogels composed of biocompatible polymers can serve as an alternative. In a one-step microgel preparation method, a cell containing prepolymer solution was confined by a thin sacrificial oil layer, which was spontaneously removed after a hydrogel matrix encapsulating the cell was formed by photo-cross-linking.[5] Besides reducing cell exposure to an oil phase, the encapsulated cells showed tissue level cell-to-cell interactions such as aggregation. Another report used hydrogels to build reliable assays to analyze islet products.[6] Encapsulated rat pancreatic islet cells outlived free islet cells during freeze−thaw processes when trehalose, a sugar believed to aid in freezing procedures, was added to the encapsulation medium before cryopreservation. In this project, ATP value, insulin secretion ability, and the oxygen consumption rate of cryopreserved encapsulated islet cells were examined to show viability and functionality improvement over cryopreserved free cells.

Beyond the encapsulation of a single cell type, picoliter printing was used to combine droplets containing different cell types into a single droplet.[7] The reported device fed a constant supply of cell containing and cell free droplets through a multiwavelength fluorescence detection zone and subsequently into an active dielectrophoretic sorter. Droplets were sorted on the basis of fluorescent signals from marked cells and then fed into a printer nozzle and dispensed to programmed positions on an oil sealed substrate. The ability to combine selected droplets under the oil allowed precise selection of cell types and control of cell numbers and reagent amounts. In another paper, a single bacterium was encapsulated in droplets on agar plates and cultured under oil.[8] The droplets were formed with a microfluidic writing device. The microdroplet system was used to examine antibiotic resistance and to identify organisms capable of degrading environmental contaminants.

Encapsulation of other biomolecule containing structures has also been an exciting topic. In an effort to create isolated systems that mimic the behavior of real cells, microscale fluidic controls were used to encapsulate multiple smaller vesicles, between 2 and 30 μm, inside of a 50 μm diameter mother vesicle.[9] Although the integrity of the smaller vesicles could be jeopardized in the flow focusing emulsion containing the mother vesicles, the system was able to compartmentalize enzymes and mimic metabolic reactions between smaller vesicles in the mother vesicle in a cell-like manner.

Transport/Sorting/Separation of Cells. The ability to transport, sort, and separate cells is critical to a wide variety of downstream capture, culture, and analysis operations on microfluidic devices. Several unique mechanical, flow, acoustic, dielectrophoretic, piezo, and centrifugal approaches have been reported to carry out these operations, some of which are highlighted below.

Mechanical Sorting. The first and the most obvious criterion for sorting cells is size. For microfluidics, physical sieve structures have been reported previously, but they have continued to evolve in terms of design to further improve the sorting of cells based on size. For example, a sequential microsieve design was reported for the improved capture of cells (Figure 1A).[10] The sequential sieves were oriented perpendicular to the flow direction with small lateral offsets so that cells would pass by occupied sieves to subsequent unoccupied ones. Retention of human breast cancer cells was demonstrated with optimized microsieve dimensions and lateral offset values. While capture specificity for differently sized cells was not shown, preferential capture of 80 μm diameter beads over 20 and 8 μm diameter beads was demonstrated. Sample throughput was not emphasized in this paper, but a substantial 7.5 mL of blood was processed in 1 h.

Other mechanical sorting devices, however, did focus on improving the throughput of cell sorting, isolation, and capture operations. For example, microsieves have been coupled to centrifugal structures to facilitate the capture of circulating tumor cells (CTCs).[11] In this device, the cell solution was focused close to the wall of a curved channel (Figure 1B). Centrifugal force caused the cells to enter small chambers lining the channel wall. The weir structures in the chambers allowed cells to be retained while the centrifugal force and applied pressure determined the size of cells captured. To retrieve collected cells, positive pressure was applied to the other end of the chambers to push out the cells. Control of the delicate equilibrium between centrifugal force and applied pressure helped to achieve a CTC purity of 100% in solutions with a CTC abundance of 1 in 20 000. The robustness and high-throughput of microsieve devices have attracted clinical interest as well. One clinical study used the Parsortix system, a commercial instrument that uses disposable separation cassettes, to screen CTCs in blood samples.[12] The step structures in the separation cassette served as size exclusion gates for the retention of CTCs above 10 μm in size. The retained cells were back flushed into a collection container for assay and microscopic analysis. This size-based commercial CTC enrichment system had a capture efficiency similar to an FDA approved immunofluorescent assay using positive EpCAM selection (CellTracker; Life Technologies).

Hydrodynamic Sorting. Hydrodynamic sorting is one the most cost-efficient ways to realize high-throughput cell sorting in microfluidic chips. In one instance, artificial flow vortices were created via chip geometry and fluidic control to trap or temporarily hold cells.[13] In this device, simple flow-through channels were coupled to multiple enlarged chambers to create vortices inside the chambers. The flow entered through a narrow inlet and proceeded through the chamber to a narrow outlet generating vortices on both sides of the flow in the chamber. The size difference between CTCs and other cells led to differences in retention within the vortexes. Although white blood cells were also captured, 5× more CTCs were captured compared to a traditional vortex chip improving the detection threshold by 5-fold. Considering the simplicity of the device and the fast flow rates achievable (2.6 mL/min), this method was competitive for fast screening and bulk cell isolation. Another vortex-based

DOI: 10.1021/acs.analchem.7b04519
Anal. Chem. 2018, 90, 65−85

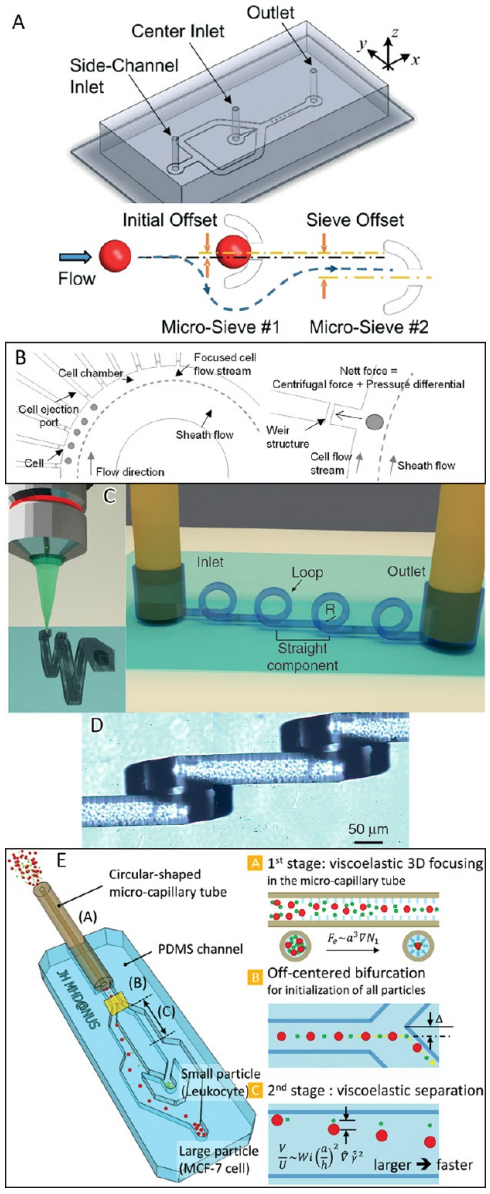

Figure 1. (A) Design of the continuous flow isolation device and diagram of the sequential microsieves showing the flow path of cells. Adapted from Tran, Q. D.; Kong, T. F.; Hu, D.; Marcos; Lam, R. H. W. *Lab Chip* **2016**, *16*, 2813−2819 (ref 10). Published by The Royal Society of Chemistry. (B) Schematic of the working principle of centrifugal microsieve trapping. Dashed line indicates interface between cell flow and sheath flow. Adapted from Yeo, T.; Tan, S. J.; Lim, C. L.; Lau, D. P. X.; Chua, Y. W.; Krisna, S. S.; Iyer, G.; Tan, G. S.; Lim, T. K. H.; Tan, D. S. W.; Lim, W.-T.; Lim, C. T. *Scientific Reports* **2016**, *6*, 22076 (ref 11). Nature Publishing Group. 3D inertial microfluidics (C and D). (C) Fabrication and structure of looped channel. (D) Microscope image of the fabricated particle focusing channel. Adapted from Paie, P.; Bragheri, F.; Di Carlo, D.; Osellame, R. *Microsystems & Nanoengineering* **2017**, *3*, 17027 (ref 16). Nature Publishing Group. (E) Schematic of sheathless capillary cell focusing and sorting device. Reprinted from Nam, J.; Tan, J. K. S.; Khoo, B. L.; Namgung, B.; Leo, H. L.; Lim, C. T.; Kim, S. *Biomicrofluidics* **2015**, *9*, 064117−064119 (ref 17), with the permission of AIP Publishing.

design used a single enlarged capture chamber and examined the trajectory of cells in the created vortex.[14] The Reynolds number was optimized to maximize the spatial separation of the trajectories for differently sized cells. The nicely separated cell trajectories could potentially be coupled to downstream detection or collection elements in the future.

In addition to using flow velocity differences to create vortices, herringbone structures are also popular for vortex generation in continuous flow microfluidic devices. One study compared cell capture using herringbone structures constructed using either sharp grooves or smooth waves to remove regions of low shear stress.[15] Both herringbone structures were coated with anti-EpCAM antibodies for affinity-based retention. Herringbone structures using sharp grooves created regions of low shear allowing the retention of nonspecific cells (purity of 25.7%) whereas the wavy herringbone structure eliminated regions of ultralow shear improving cell purity to 39.4% while maintaining high capturing efficiency (>85%). Besides nonspecific retention, the smooth surface also reduced high shear regions, which were harmful to cell viability. Cell viability was 11% higher for the wavy herringbone structure compared to the grooved herringbone structure.

Hydrodynamic Focusing. Hydrodynamic focusing of cells can be carried out using specially designed chip geometries and flow manipulation using a variety of approaches on microfluidic devices. For example, micrometer-sized, three-dimensional devices that consisted of sequential loops were fabricated via femtosecond laser exposure and wet etching (Figure 1C,D).[16] At a radius of several hundred micrometers, these loops facilitated particle focusing over a broad range of sizes by inertial effects and asymmetric Dean flow. This novel fabrication method achieved focusing without a sheath flow. For many focusing applications, sheathless flow is an alluring feature in terms of creating a simple, compact device. Another sheathless focusing report used a capillary−PDMS hybrid device to focus leukocytes and MCF-7 cells (Figure 1E).[17] Cells flowed out of the capillary and into the base part of a Y-shaped microfluidic channel in a focused manner. The focused cells were deflected at the bifurcation point in the channel and subsequently flowed along different trajectories based on size-induced elastic force differences (Figure 1E). As a demonstration, MCF-7 cancer cells were separated from leukocytes with a final purity close to 100%.

The use of sheath flow, however, still offers an advantage over sheathless flow as it can perform focusing at higher flow rates. A multilayer glass device used both vertical and lateral sheath flows for high-throughput sample focusing.[18] At linear velocities from 0.7 to 10 m/s (or volumetric flow rates of 10−60 μL/min), the cell flow was confined inside a 10 × 10 μm cross-sectional area close to single cell dimensions. Importantly, this device was comparable in throughput to benchtop scale flow cytometers.

Acoustic Focusing. In our last review, surface acoustic waves (SAW) received attention in sorting applications as a non-invasive, contactless, label-free technology. Most SAW sorting projects utilize a set of coupled transducers on a piezoelectric substrate to generate acoustic waves resulting in 2D lateral displacement in a focused flow. To improve flow focusing, a recent paper demonstrated three-dimensional manipulation with two sets of transducers using phase shift for horizontal control and amplitude for vertical control.[19] By tuning the displacement node position in the interfering SAW network, living cells were lined up and moved at an average speed of 2.5 μm/s. This development opens possibilities for the creation of complicated cell sorting and collection chip structures. Despite the capability of 3-dimensional manipulation, 2-dimensional sorting has been popular due to the ease of integration of the electrodes with single-layer microchips. One example of this type of device includes active SAW sorting with fluorescence interrogation

DOI: 10.1021/acs.analchem.7b04519
Anal. Chem. 2018, 90, 65−85

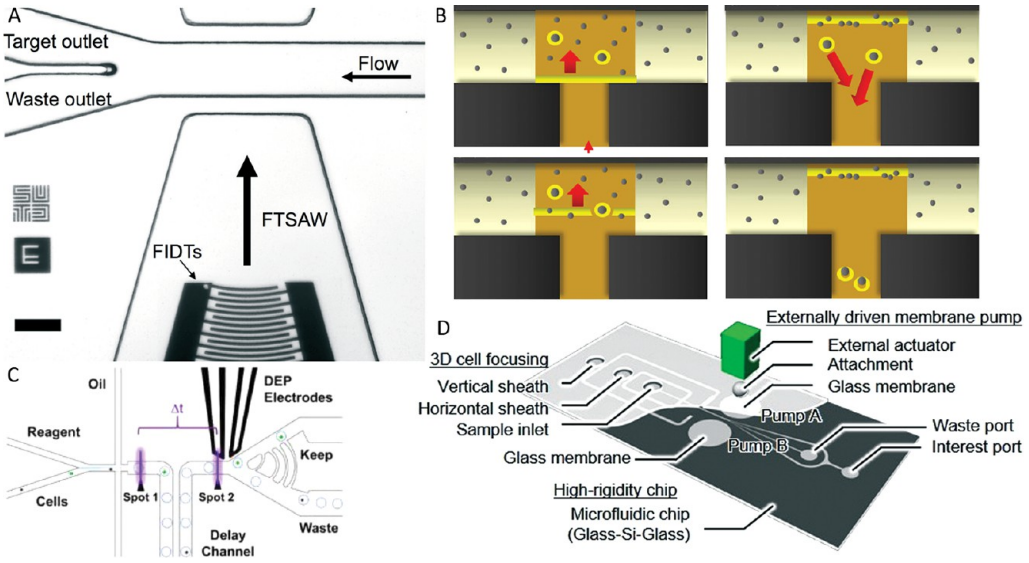

Figure 2. (A) Focused interdigital transducer for active fluorescence sorting. Adapted from Ma, Z.; Zhou, Y.; Collins, D. J.; Ai, Y. *Lab Chip* **2017**, 3176−3185 (ref 20), with permission of The Royal Society of Chemistry. (B) Targeted cancer cells trapped and moved by light rings and other cells excluded by a light bar due to optical-induced-dielectrophoresis. Adapted from Chiu, T.-K.; Chou, W.-P.; Huang, S.-B.; Wang, H.-M.; Lin, Y.-C.; Hsieh, C.-H.; Wu, M.-H. *Scientific Reports* **2016**, *6*, 32851 (ref 24). Nature Publishing Group. (C) Two spot LIF monitoring of transient cellular responses of genetically encoded FRET responder and active DEP sorting. Adapted from Fiedler, B. L.; Van Buskirk, S.; Carter, K. P.; Qin, Y.; Carpenter, M. C.; Palmer, A. E.; Jimenez, R. *Analytical Chemistry* **2017**, *89*, 711−719 (ref 29). Copyright 2017 American Chemical Society. (D) Active cell sorting by dual membrane pumps controlled by piezoelectric actuators. Adapted from Sakuma, S.; Kasai, Y.; Hayakawa, T.; Arai, F. *Lab Chip* **2017**, *17*, 2760−2767 (ref 30), with permission of The Royal Society of Chemistry.

(Figure 2A).[20] In this work, MCF-7 cells were fluorescently stained and mixed with diluted human whole blood. Sandwiched by two sheath flows, the mixture was interrogated at a 70 μm diameter laser spot. Fluorescence emission from labeled MCF-7 cells triggered an AC pulse to a SAW transducer to divert selected cells for isolation. Purities of 80−90% were achieved for the collected cells with over a 90% recovery of spiked MCF-7 cells.

Centrifugation. Centrifugal microfluidics differentiate cells by size and density. In clinical settings, cells in blood with various densities have been traditionally separated via centrifugation. In order to improve such separations, a gradient generating medium was added to a centrifugal microchip.[21] The PDMS-based microchip was first pretreated with a blocker reagent to reduce surface interaction and then filled with a blood sample and density gradient medium. Immune cells were successfully separated in an optimized chip structure under spinning conditions. Viability tests of the separated cells showed viability and function were still comparable to that of the original sample. Instrumentation for centrifugal sorting is relatively simple, as it requires little more than a controllable spinner. One group developed a centrifugal microchip with a custom fabricated benchtop spinning platform that included a spinning bucket into which a microchip could be placed.[22] When a solution was flowed through the separation channel under spinning conditions, the centrifugal force drove particles of different densities to different depths in the channel. MCF-7 cells spiked into diluted whole blood samples were separated using the device with an efficiency of around 75%.

Dielectrophoresis. Dielectrophoresis (DEP) has been a popular cell sorting method due to its strong driving force and facile integration with other components. Depending on the polarizability of cells in the medium, DEP can be divided into two modes: cell attracting (positive DEP) and cell repulsing (negative DEP). One example of a device for carrying out insulator-based dielectrophoresis used a one-layer PDMS chip with insulating posts.[23] Fluorescent polystyrene beads with diameters of 500 nm and 1 and 2 μm as well as yeast cells were moved using electroosmotic flow and captured between insulator posts. The capture capabilities of this device were shown by mixing yeast cells with 500 nm beads in a concentration close to that of CTCs in blood. The capture efficiency was over 90%. Another CTC sorting method relied on active manipulation via optically induced dielectrophoresis (ODPE) to improve CTC isolation results from whole blood.[24] The red and white blood cells were removed using commercially available negative selection kits. After negative selection, the remaining cells were loaded onto a microfluidic device and pulled past an ITO electrode connected to a function generator applying an electric field. When cells arrived at the ITO electrode, flow was temporarily stopped and fluorescence images were collected to distinguish labeled CTCs from leukocytes and other cells. Then, a computer controlled light projection device was used to enclose the CTCs in a light ring and preclude other cells with a light bar (Figure 2B). The ring-enclosed CTCs were then moved into a collection channel while the rest of the cells were kept inside the main channel. This method offered CTC collection purity up to 100% and a cell recovery rate of 41.5%. Another work incorporated an inline size exclusion filter to remove red blood cells in the sample prior to DEP.[25] The remaining mixture of white blood cells and prostate cancer cells was transported to DEP electrodes where the prostate cancer cells were selectively captured for further analysis.

Novel electrode materials for DEP enrichment and capture using carbon nanofibers have also been reported.[26] For example, a 200 μm × 200 μm array containing carbon nanofiber electrodes was placed inside a microfluidic flow chamber. An *E. coli* containing solution was fed to the array where *E. coli* were captured through the application of a mild AC field. The limit of detection for *E. coli* was 210 CFU/mL using a commercial, portable Raman system. Although *E. coli* recovery from

DOI: 10.1021/acs.analchem.7b04519
Anal. Chem. 2018, 90, 65−85

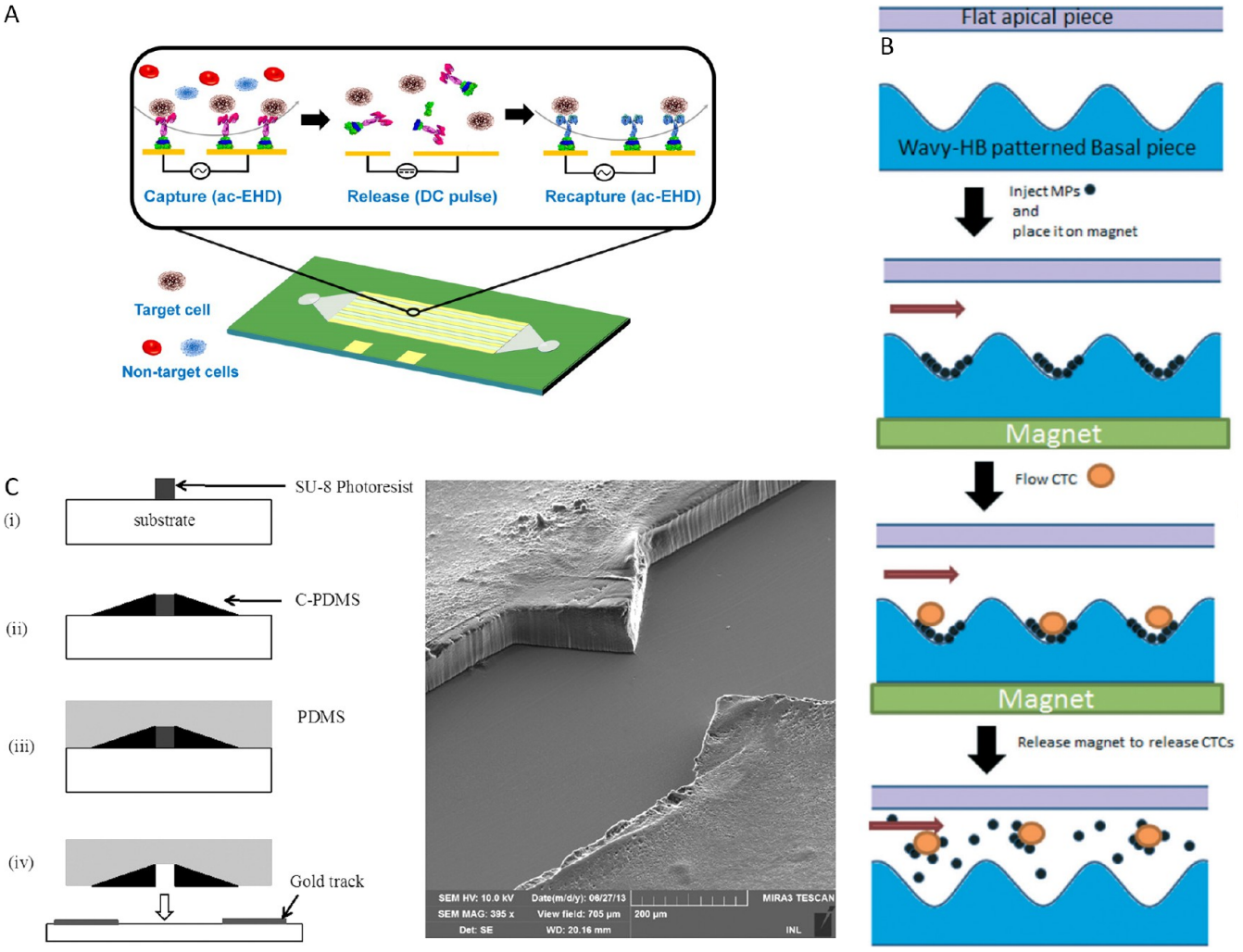

Figure 3. (A) Electric field induced cell capture, release, and recapture. Adapted from Dey, S.; Vaidyanathan, R.; Carrascosa, L. G.; Shiddiky, M. J. A.; Trau, M. *ACS Sensors* **2016**, *1*, 399−405 (ref 32). Copyright 2016 American Chemical Society. (B) Experimental steps of magnetic CTC capture and release. Adapted from Shi, W.; Wang, S.; Maarouf, A.; Uhl, C. G.; He, R.; Yunus, D.; Liu, Y. *Lab Chip* **2017** (ref 33), with permission of The Royal Society of Chemistry. (C) Fabrication process of thick electrodes and SEM image of C-PDMS electrodes before sealing. Reprinted from Marchalot, J.; Chateaux, J.-F.; Faivre, M.; Ferrigno, R.; Deman, A.-L.; Mertani, H. C. *Biomicrofluidics* **2015**, *9*, 054104 (ref 36), with the permission of AIP Publishing.

complicated sample matrices such as a soil solution was estimated at 15%, single *E. coli* capture could be detected by the carbon nanofiber array electrodes.

While positive DEP can be used to attract and sort particles with higher polarizability, negative DEP can be used to repel targeted particles. One work incorporated negative DEP with a hydrodynamic filter to attain cell free plasma from whole blood.[27] The microfluidic chip was designed with a main flow channel for whole blood and a size exclusion hydrodynamic filter. The hydrodynamic filter was aligned with DEP electrodes to repel cells to prevent clogging of the filter.

Encapsulated Droplet Sorting. Droplet microfluidics are commonly used to segregate single cells to create an isolated environment for reaction and signal readout. The ability to distinguish encapsulated single cells and sort them in a high-throughput manner is critical for the success of this endeavor. One study incorporated PCR with single cell droplet sorting to achieve cultivation-free identification of a virus host.[28] Virus infected bacteria were first encapsulated with a PCR primer and a TaqMan probe, which released fluorescent dye during PCR amplification of the targeted sequence. Encapsulated bacteria then underwent thermocycling for bacterial lysis and PCR amplification. After PCR, droplets were interrogated on the basis of the fluorescence and were subsequently sorted and collected using DEP. DNA could then be harvested from collected cells for further analysis using qPCR. This method allowed screening and collection of infected host cells at several kHz while still allowing further quantification of the DNA in the droplets by qPCR. While throughput is important, other studies focused on using the droplets to monitor reactions. Cells genetically encoded with a fluorescence resonance energy transfer (FRET) pair containing two fluorescent proteins were encapsulated with a reactant Zn^{2+} solution and monitored for changes in fluorescent signal.[29] In the unreacted state, one fluorescent protein was quenched, and in the reacted state, the other protein was quenched. The transition of this FRET pair from unreacted to reacted state was monitored using two detection points in the droplet channel (Figure 2C). Cells that showed expression of both proteins and underwent transition in fluorescence were sorted out by DEP. This helped to enrich the fluorescent protein expressing cells from 10% in the whole mixture to a purity of over 90% after sorting.

Piezopump Sorting. Piezo actuators can displace nanoliter volumes of fluids at frequencies in the kHz range making them great tools for manipulating cells. In one report, piezo actuators

DOI: 10.1021/acs.analchem.7b04519
Anal. Chem. 2018, 90, 65−85

were attached to a glass membrane on top of solution storage chambers connected to a microfluidic cell sorting channel manifold (Figure 2D).[30] As glass is a rigid material, the actuation frequency that could be applied was higher than that for elastic materials, such as PDMS. Using these piezoelectric pumps, fluid flow from the chambers into the microfluidic channel could be quickly adjusted to redirect cells at the channel outlet. The reported device incorporated fluorescence interrogation to send signals to the actuator for the active sorting of cells of interest. Cells could be interrogated and collected at tens of kHz with recovery rates and collection purities of over 90%.

Cell Capture. Often, the next step in the analysis of cells on microfluidic devices is the selective capture of cells at specific locations. These captured cells can then be studied to examine long-term drug responses, intercellular interactions, and the effects of other external perturbations. The three most popular methods of capture in the last couple of years have been affinity, dielectrophoretic, and acoustic based.

Affinity-Based Capture. Affinity-based interactions are very specific, involving the interaction of some ligand with a specific binding partner. The most commonly used affinity method, immunoaffinity, takes advantage of antibody−antigen interactions. The main challenges associated with this technique include nonspecific binding, real-time capture monitoring, and release of captured cells without damaging them. A common immunocapture approach for cells uses anti-EpCAM antibodies, as EpCAM is overexpressed in many epithelial derived cancers and thus found on many types of CTCs. Efficient isolation of very low abundance CTCs can help improve disease diagnosis. Microfluidic devices have served as robust platforms for the capture and isolation of CTCs. In one recent report, a bionic TiO_2 inverse opal photonic crystal (IOPC) conjugated to anti-EpCAM antibodies through polydopamine was used to capture magnetic bead labeled CTCs in a glass microfluidic device.[31] The capture efficiency for CTCs on the IOPC interface was higher by a factor of 20 compared to capture on flat glass. The CTC capture efficiency in blood was >60% with a 1 mL/h flow rate at an abundance of 200 CTCs per mL. The optical properties of the IOPC also enhanced the fluorescence emission by 35% to more easily monitor the capture of CTCs. In another device, subpopulations of tumor cells were identified using a double capture affinity microfluidic chip with alternating current electrohydrodynamic flow.[32] In this device, cells were initially captured using an anti-EpCAM antibody, released by switching from AC to DC current, and then recaptured using an antihuman epidermal growth factor receptor 2 (HER2) antibody as shown in Figure 3A. The capture efficiency for the anti-EPCAM was 64.8 ± 2.6%, followed by an 84.5 ± 3.2% release success, and then a 42.9 ± 2.4% capture efficiency for anti-HER2. A third reported device used a wavy-herringbone structured channel molded in PDMS to capture and release CTCs on anti-EpCAM coated magnetic particles.[33] The device created passive turbulence and increased the probability of tumor cells colliding with the device wall where they were captured. By removing the magnetic field, the captured cells with a surplus of magnetic particles were released from the device and collected (Figure 3B). The capture efficiency of CTCs from whole blood samples was 81−95%. To identify and separate CTCs, one report presented magnetic nanoparticles linked to anti-EpCAM.[34] The quantity of magnetic nanoparticles that attached to the cells was a function of the cells' EpCAM expression level. On the basis of retention caused by an external magnetic field, cells were sequentially separated into four groups representing the relative expression levels of EpCAM. Differences in EpCAM expression among the cells were shown to be related to collagen uptake and invasiveness. Human Transferrin Receptor is another antibody that has been used to select specific cell types on a microfluidic device.[35] These antibodies were attached to a herringbone-patterned channel that both increased the surface area and created passive turbulence. The device was used to detect acute lymphocytic leukemia. The leukemia cells were spiked into blood and isolated with 82−97% purity. Patient-derived ALL cell lines COG-LL-332 and COG-LL-317 were isolated in the chip with 80−97% and 57−92% purity, respectively. Initial spiked concentrations were as low as 1%.

Dielectrophoretic-Based Capture. There have been several reports that integrate microelectrodes into microfluidic devices to dielectrophoretically trap single cells. DEP trapping makes use of a cell's response to an asymmetrical electric field to capture it above an electrode. In some cases, different types of cells, even with similar shape or size, can be selectively captured without requiring biochemical or magnetic labeling. For example, a polymeric microfluidic device was developed with integrated thick carbon nanoparticle−PDMS composite electrodes designed to carry out DEP trapping of low abundance biological cells (Figure 3C).[36] Trapping efficiencies with the MDA-MB-231 breast cancer cell line reached 97%, but the volumetric flow rates through the device were very low. A second paper reported the use of octupole electrodes for negative DEP trapping of nine different cell types, including bacteria, yeast, platelets, and cancer cells.[37] A variety of different applications for this contactless capture method were demonstrated including the examination of elasto-mechanic properties of the captured cell, the perfusion of perturbation agents, and proximity-based cell−cell interactions. This method, as with the previous method, suffered from very low throughput and so would be best coupled to other enrichment methods.

Exosome Capture. Exosomes have become quite a popular target for single-cell analysis. Exosomes are small extracellular vesicles (EVs) that contain proteins and nucleic acids from their originating cells and play vital roles in intercellular communication. Commonly, immunocapture is used to separate and study them in microfluidic devices. One group used a viscoelasticity-based PDMS microfluidic system to directly separate exosomes from cell culture media or serum in a continuous, size-dependent, and label-free manner.[38] Using a small amount of poly(oxyethylene) as the additive in the media to control the viscoelastic forces exerted on EVs, they achieved a high separation purity (>90%) and recovery (>80%) of particles <200 nm in size. Another exosome isolation device used a unique coating of graphene oxide and polydopamine for ultrasensitive detection via an ELISA assay.[39] Two μL of plasma were used without preprocessing. The LOD was 50 exosomes/μL with a 4 log dynamic range, and the assay was able to discriminate ovarian cancer patient exosomes from healthy controls. A third very interesting microfluidic device was fabricated with an array of PDMS micropillars that were chemically functionalized with multiwalled carbon nanotubes (MWCNT).[40] The CNT interfaces were coated with an antiavidin antibody. These antibodies captured avidin labeled exosomes from cells that were biotinylated and filled with a specific drug. The captured exosomes contained some of the drug. Once the exosomes were released, they could be used as delivery vehicles for the drugs to other cells. A purified exosome delivery system for tumor drugs could improve cancer treatments and drug efficiency due to dual ligand targeting and receptor-mediated endocytosis.

DOI: 10.1021/acs.analchem.7b04519
Anal. Chem. 2018, 90, 65−85

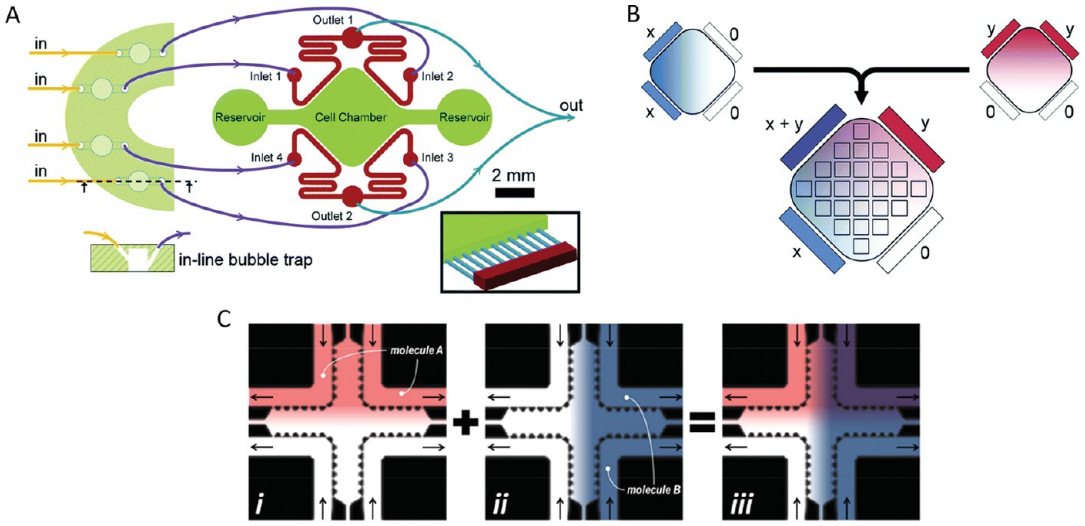

Figure 4. Cell culture with gradient generator (A and B). (A) Schematic of cell chamber and parallel reagent channels interconnected by microchannels (inset). (B) Principle of orthogonal gradient generation. Adapted from Kilinc, D.; Schwab, J.; Rampini, S.; Ikpekha, O. W.; Thampi, A.; Blasiak, A.; Li, P.; Schwamborn, R.; Kolch, W.; Matallanas, D.; Lee, G. U. *Integrative biology: quantitative biosciences from nano to macro* **2016**, *8*, 39−49 (ref 50), with permission of The Royal Society of Chemistry. (C) Formation of two concentration gradients orthogonal to each other. Adapted with permission from Uzel, S. G. M.; Amadi, O. C.; Pearl, T. M.; Lee, R. T.; So, P. T. C.; Kamm, R. D. *Small* **2016**, *12*, 612−622 (ref 51). Copyright 2015 Wiley-VCH Verlag GmbH & Co. KGaA, Weinheim.

Another microfluidic device used multiple inlets, serpentine channels, and reaction chambers to capture circulating EpCAM-positive exosomes using immunomagnetic particles.[41] Exosomes from 6 breast cancer patients and 3 healthy controls were examined using this device. In the breast cancer patients, there was a 2-fold increase in the EpCAM-positive exosomes, compared to healthy controls. Circulating HER2-positive exosomes from 19 breast cancer patients' samples were also quantified, and the exosomal HER2 expression levels were consistent with those in tumor tissues assessed by immunohistochemical staining. Immunomagnetic beads were also used in a PDMS-based continuous-flow microfluidic device to isolate exosomes from blood plasma for in situ multiplexed detection.[42] A blood-based diagnostic device for ovarian cancer was developed using a multiplexed measurement of three exosomal tumor markers (CA-125, EpCAM, CD24) and a training set of ovarian cancer patient plasma samples. This device showed significant diagnostic power (a.u.c. = 1.0, p = 0.001) and was comparable with the standard Bradford assay.

While most methods to capture exosomes involve affinity interactions, a nonimmunoaffinity method to capture exosomes based upon acoustofluidics was also reported.[43] This platform consisted of a microscale cell-removal module that first removed larger blood components, followed by extracellular vesicle separation. This two-module separation could isolate exosomes from 100 μL of undiluted human blood within ∼25 min. The exosomes were isolated with a purity of ∼98% and a yield of ∼82%.

CELL CULTURING AND ANALYSIS OF INTACT CELLS

A broad range of devices for culturing and analyzing cells in microfluidic devices have been reported including those focused on simple monocultures, more complex cocultures, sophisticated 3-dimensional tissue models, and finally almost complete physiological models. Both eukaryotic and prokaryotic cells have been cultured. A wide variety of parameters in these cultures have been measured in response to various chemical and physical perturbations. In this section, we first focus on basic improvements to cell culturing and analysis on chip and then move to more complex multicell type culturing and analysis systems.

Single Cell Type Culturing and Analysis. A particular advantage of culturing cells in microfluidic devices is the ability to integrate sensors, especially light- and electrical-based sensors, directly into the cell culture chamber. One example includes the integration of an impedimetric sensor array to measure bacterial biofilm growth.[44] In this paper, the authors reported a smart, threshold activated impedance-based feedback sensor to detect the growth of *E. coli* biofilms. In addition to detection, however, they also demonstrated that the same electrodes could be used to kill the biofilm using what they called the bioelectric effect. This treatment resulted in a ∼75% reduction in biofilm area compared to untreated negative controls. A similar sensing system was used to monitor cell response to acute and chronic nanoparticle exposure.[45] In another on-chip cell culture system, a series of thin-film sensors were integrated into a PDMS−glass device to measure respiration, pH, and cell adhesion.[46] These parameters were monitored in mouse-embryonic/fetal calvaria fibroblast cells using an amperometric oxygen electrode, a potentiometric pH electrode, and an interdigitated electrode array to examine adhesion. Another reported an O_2 measuring method used luminescence in a microfluidic paper-based cell culture system.[47] For this system, a luminescent polystyrene film containing Pd(II)tetrakis(pentafluorophenyl)-porphyrin dye was used. The film was shown to be stable and nontoxic with a linear response to O_2 from 0 to 160 mmHg.

As a general rule of thumb, it is critical to be able to determine whether cells that are being cultured are alive, apoptotic, or dead. In a recent paper, a novel simplified one-step continuous process to monitor cell health was reported using propidium iodide and counterstains.[48] These dyes were introduced in a noninvasive manner at nontoxic levels into a multiwell microfluidic culturing system.[49] Results demonstrating its effectiveness were reported. This approach could be applied to monitoring cell health in a wide variety of microfluidic culturing systems. The relevance of the ability to track the condition of cells during culture was

DOI: 10.1021/acs.analchem.7b04519
Anal. Chem. 2018, 90, 65−85

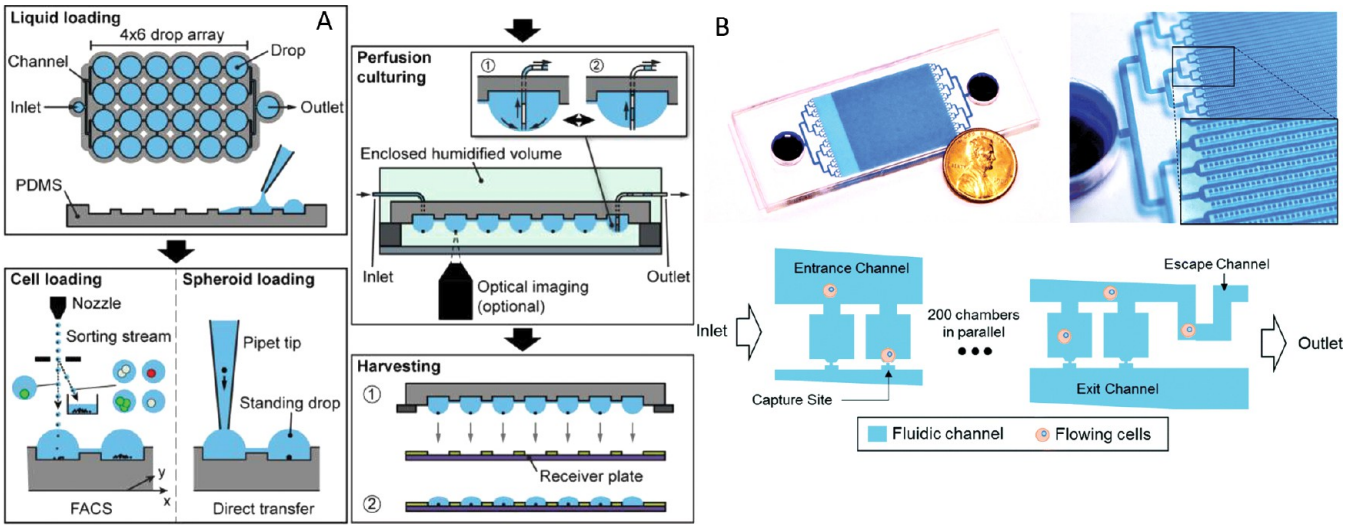

Figure 5. (A) Layout and workflow of hanging-drop network cell culturing. Adapted from Birchler, A.; Berger, M.; Jaggin, V.; Lopes, T.; Etzrodt, M.; Misun, P. M.; Pena-Francesch, M.; Schroeder, T.; Hierlemann, A.; Frey, O. *Analytical Chemistry* **2016**, *88*, 1222−1229 (ref 56). Copyright 2016 American Chemical Society. (B) Top: Image and close-up of a flow-through cell culture array with 12 800 chambers. Bottom: Schematic of single branch channel. Adapted from Cheng, Y.-H.; Chen, Y.-C.; Brien, R.; Yoon, E. *Lab Chip* **2016**, *16*, 3708−3717 (ref 58), with permission of The Royal Society of Chemistry.

shown in a device used to examine the interaction of MEK and EGFR pathways in breast cancer cells.[50] In this device, linear combinations of MEK and EGFR inhibitors were generated in a microfluidic cell culture chamber, in part to examine their interactions in apoptotic signaling (Figure 4A,B). The generation of stable gradients in linear combinations allowed the quick assessment of the interactions between the two signaling inhibitors in lieu of expensive and time-consuming titration experiments. The motility and morphology of the cells were also examined in the experiment. In addition to a better understanding of the effects of molecular gradients on apoptosis, biochemical gradients are also a useful tool in the study of cell differentiation and cell migration. A second device using a different design than that described above was also used to create linear diffusion driven gradients of two signaling molecules (Figure 4C).[51] The gradients could be applied in sequential, orthogonal, or linear combinations to a 3D cell-embedded scaffold. The gradient direction could also be rotated about the central point in the chamber. Differentiation of stem cells and the directional motility of cancer cells in response to the gradients were examined. A simpler glass device with a Y shaped channel manifold was commercially purchased from Ibidi to perform a chemotaxis assay.[52] A stable gradient of an EGFR stimulator was set up across the base channel of the device, and the motility of >6600 breast cancer cells was measured. This paper is instructive in that it shows how microfluidics has moved out of the research lab, and now, commercially available devices can be used off the shelf in biology laboratories. In addition to gaining a better understanding of how EGFR's affect cell physiology, microfluidic cell culturing devices can also be used to gain a better understanding of how ligands bind to such receptors. For example, a microfluidic device for single molecule imaging of subcellular sections was reported.[53] In this device, a silicon nitride nanoaperture zero mode waveguide array was used to isolate small sections of a cell to allow the real-time measurement of single ligands binding to EGFRs. The apertures were ∼200 nm in diameter, and the ligands were delivered through PDMS microchannels in which the cells were being cultured on the nanoaperture arrays.

The use of biological gradients, as shown above, provides differentiation cues to cells. In addition to biological signaling molecule cues, shear stresses can provide cues that can change the functionality of cells and generate differentiation. A device to examine the transition of murine myoblast cells to myotubes was reported.[54] In this PMMA-based device, a series of laser-cut constant-width parallel channels was fabricated. The channels varied in width from 2 mm to 100 μm in 100 μm steps and were coated with Type-I collagen to culture the cells. The volumetric flow rate into each channel was the same so shear stresses were higher in the narrower channels. The concentrations of myogenic mRNA biomarkers were shown to increase under 16 mPa shear flow compared to static conditions.

Cells, as living organisms, both consume nutrients and produce waste; therefore, cell culture systems must be continually resupplied with nutrients and flushed of wastes. As such, most microfluidic cell culture systems integrate some type of pumping, often using a pump external to the chip itself. In order to try to create a low-cost, disposable, small footprint device, a unique hydrophobic/hydrophilic patterning technique using a fluorosilanized UV-independent TiO_2 nanoparticle coating has been reported.[55] In this wedge-shaped culturing device, bacterial and eukaryotic cells were successfully patterned in the hydrophilic wedge between the hydrophobic walls. Eukaryotic cell viability was >97.5% after 48 h. One particular advantage of this device was that the cells remained accessible throughout the experiment due to the open device design. The ability to directly access cells has many advantages in terms of both loading them into the device and harvesting them. Another open microfluidic system was reported that used hanging drops in a humidified chamber to allow easy access to the cells.[56] In this system, an array of open wells interconnected with microfluidic channels was loaded with single cells (or tissue spheroids) using the exit nozzle from a fluorescence-activated cell sorter or a pipet tip. The array was then flipped over to create perfused hanging drops in a humidified chamber (Figure 5A). The drops could be imaged, and cells were harvested by touching the drops to a receiver plate. A variety of cell types were cultured for 5 days, and fluorescence-based assays to monitor the cells were performed.

DOI: 10.1021/acs.analchem.7b04519
Anal. Chem. 2018, 90, 65−85

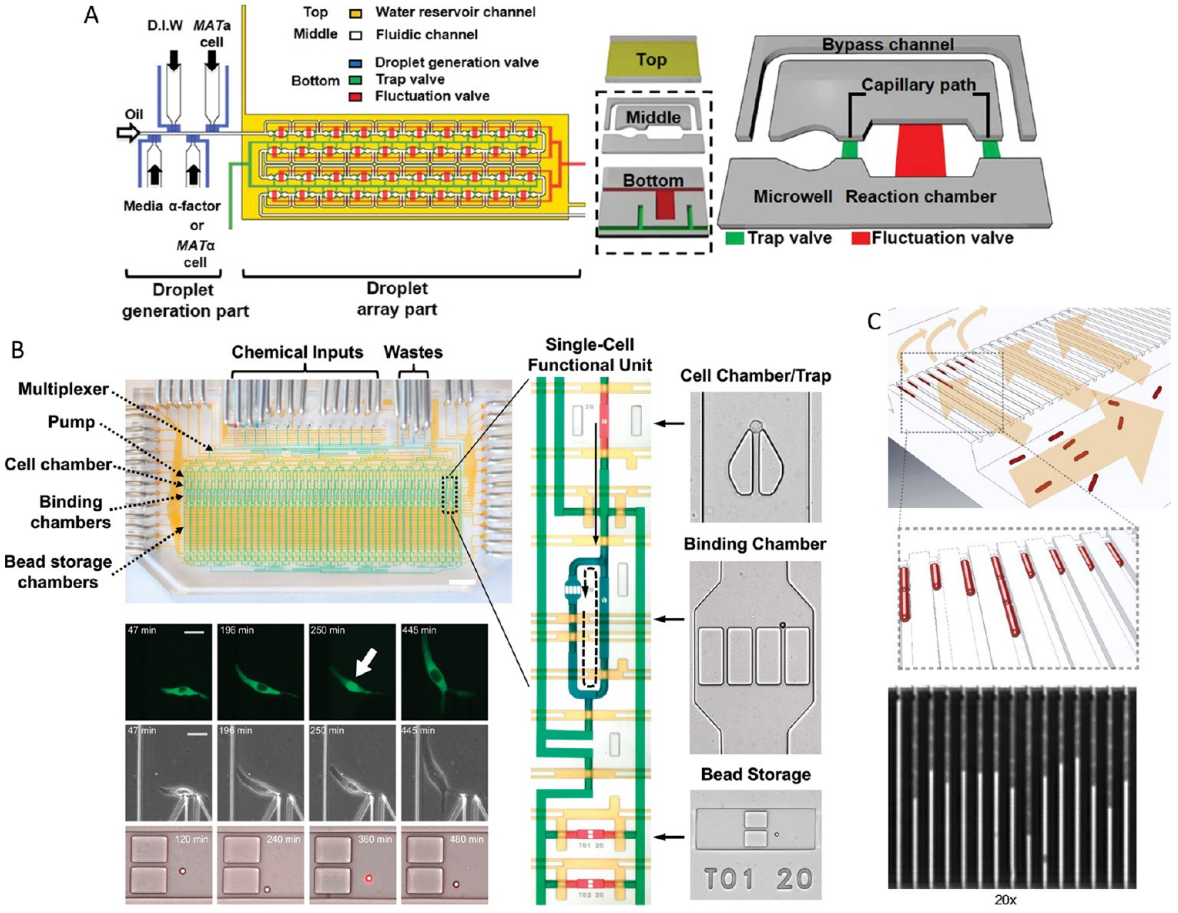

Figure 6. (A) Schematic diagram of the microfluidic droplet trapping array and a single unit of the hydrodynamic trap. Adapted from Jin, S. H.; Lee, S. S.; Lee, B.; Jeong, S.-G.; Peter, M.; Lee, C.-S. *Analytical Chemistry* **2017**, *89*, 9722−9729 (ref 59). Copyright 2017 American Chemical Society. (B) Photograph of the automated nanoliter immunoassay with functional areas indicated and an enlargement of a single functional column. Reprinted from Junkin, M.; Kaestli, A. J.; Cheng, Z.; Jordi, C.; Albayrak, C.; Hoffmann, A.; Tay, S. *Cell Reports* **2016**, *15*, 411−422 (ref 62), from Elsevier. DOI: 10.1016/j.celrep.2016.03.033 (https://creativecommons.org/licenses/by-nc-nd/4.0/). (C) Top: Cartoon illustrating the trapping of rod-shaped bacterial cells for antibiotic susceptibility examination. Bottom: Phase contrast image of trapped *E. coli*. Adapted from Baltekin, O.; Boucharin, A.; Tano, E.; Andersson, D. I.; Elf, J. *Proc. Natl. Acad. Sci U.S.A.* **2017**, *114*, 9170−9175 (ref 66). Copyright 2017.

Another potential approach to culturing cells on microfluidic devices with open access is to use paper as the substrate material. The design of most paper devices, however, is not compatible with a continuous perfusion of liquid because, as the paper channel becomes saturated with liquid, flow decreases and then stops. In order to continuously perfuse the paper, a method to remove (absorb) the liquid is needed. Recently, a microfluidic paper-based analytical device (μPAD) was reported that was designed to continuously perfuse the paper by connecting the μPAD to a media source on one side and an absorption sink on the other side.[57] A cell-laden hydrogel solution was applied to the paper, and the device was placed in a cell culture chamber. Mouse fibroblast cells were cultured for 7 days on this device, and a drug-screening assay using paclitaxel was demonstrated.

The ability to just culture cells in a microfluidic device is often not sufficient as one may also need to specifically track individual cells or cell lineages to examine how they respond to specific perturbations and to measure the potential heterogeneity of responses. For example, a microfluidic device was reported to capture and culture a representative sample of cancer-like stem cells.[58] This device consisted of over 12 000 individual cell capture units arrayed in a way such that the flow through a single capture unit was blocked by a captured cell thus sending subsequent cells downstream to the next capture unit and so forth (Figure 5B). The captured cells could be cultured for over 2 weeks. An automated image acquisition and analysis program tracked the development of 10 000 cells in the device over time. Results from the cell culture experiments showed considerable heterogeneity in the growth, reproduction, and spheroid forming capability of these cells, which was hypothesized to possibly be reflective of their ability to metastasize.

Another method that can be used to keep track of specific cells involves trapping the cells in droplets. In one report, a sophisticated microfluidic device was used to develop a better understanding of cell−cell communication among yeast cells in droplets (Figure 6A).[59] This device created water-in-oil droplets containing cells that were then captured in one of 40 hydrodynamic traps in the main device. Using soft lithographic valves, the delivery of additional reagents to the yeast containing droplets could be controlled. This device was used to measure how budding yeasts responded to peptide mating pheromones and was found to provide higher accuracy results than conventional methods. In a creative twist on cell encapsulation to study cell−cell communication, yeast and bacteria were encapsulated into single droplets on a microfluidic device to produce a transcription factor-based biosensor.[60] The yeasts were genetically modified to produce a product that would cause the genetically modified bacteria to produce yellow fluorescent

DOI: 10.1021/acs.analchem.7b04519
Anal. Chem. 2018, 90, 65−85

protein. Yeasts that were high producers could then be rapidly sorted from low and nonproducers. Another approach to analyzing the production from genetically modified organisms is to directly measure the product produced. In an interesting application, a microfluidic cell culturing device was used to monitor enantioselective biotransformations.[61] This device integrated the culturing of *E. coli* cells expressing an epoxide hydrolase with a chiral electrophoretic separation and deep-UV time-resolved fluorescence detection of the product.

Another complex, automated microfluidic device for multiparameter analysis of single-cell immune dynamics was also recently reported.[62] This PDMS-based device integrated a series of sieve-based cell capture structures in which to culture a variety of cell types and chambers to store reporter beads used to monitor cytokine expression from the captured cells.(Figure 6B) The cell and reporter bead transport and capture were automated. The reporter beads were moved to sample the cell media efflux from a specific cell at certain time intervals and then moved back to a storage site for readout. The cells were stimulated, and individual cell responses were monitored automatically over long periods of time. In a much simpler device, the differential migratory behaviors of immune cells were examined in the context of chemotherapy-induced antitumor immunity.[63] In this device, the migration of mouse splenocytes and peripheral blood mononuclear cells (PBMC) toward dead or dying cells that had been treated with doxorubicin was examined as a function of whether the splenocytes or PBMCs expressed functional FPR1.

The ability to track the individual growth of single-celled organisms such as bacteria and yeasts can lead to better insights into changes in growth due to genetic manipulation, antibiotic resistance, and general aging. For example, a multiheight PDMS−glass hybrid device was reported to measure the effects of gene deletions on *E. coli* growth.[64] In this device, bacteria were loaded at low densities and were trapped in a pillar-supported area between two larger channels through which media flowed. The growth of colonies from single cells was followed via imaging. A similar PDMS-based device was also used to track slow growing cyanobacteria in a chamber isolated with integrated soft lithographic valves.[65] Cell growth for these bacteria was shown to only occur during the light part of the light−dark cycle, and cell division occurred after a constant increase in cell volume. A more sophisticated device to trap bacteria at specific locations was reported to examine the susceptibility of bacteria to antibiotics.[66] In this PDMS−glass hybrid device, an array of 2000 capture channels was fabricated to trap single bacterium as they flowed through the channels (Figure 6C). The bacteria were then treated with antibiotics, and the growth rate was monitored through visual imaging. Differences in growth rates for antibiotic resistant and susceptible bacteria could be distinguished within 10 min. The entire test from loading to end could be completed within 30 min. The device was tested using 49 uropathogenic *E. coli* isolates and correctly identified each as either susceptible or resistant. A similar PDMS−glass device was also reported for capturing bacteria.[67] This device was used for longer-term observation of bacterial growth through many generations for up to 20 h. A third device using similar design principles was used to trap 1500 individual yeast cells and monitor growth over up to 80 generations.[68] Experiments with the yeast showed that protein aggregates could not be used as a marker for replicative aging.

Analysis of Cocultures. One of the most exciting and hottest areas in microfluidic-based cellular analysis is in the development of coculturing systems. Most of this interest is driven by the desire to better understand cell−cell communication and how pharmaceuticals are metabolized in the body and affect various (off-target) cell types.

There are several ways in which to generate cocultures in microfluidic devices. In many cases, the cocultures need to be initially or permanently separated by some type of barrier, oftentimes a permeable barrier. An interesting example of how to create an inexpensive and simple impermeable barrier is the use of a monofilament fishing line to divide a cell culture chamber into two or more parallel sections.[69] The monofilament line could be slid out of the PDMS chamber through channels with minimal hydrodynamic disturbance to restore the connections. While inserted, the filament provided a tight seal between the chambers and the isolated sections could be coated with different surface materials or seeded with different cell cultures through access channels. A coculture of neurons and glial cells was demonstrated. The specific patterning of cells for coculture has also been shown using benzophenone cross-linked through UV irradiation.[70] Using this approach, cells and benzophenone were added to a microfluidic channel and a section of the channel was irradiated to cross-link the benzophenone and trap the cells. The untrapped cells could then be flushed and another cell type added, and the process, repeated in a section of the channel near the previously trapped cells thus creating a coculture. The UV-irradiation caused little cell death, and patterned cocultures ∼200 μm in diameter with 200 μm spacings were produced. Cells were shown to be alive after 24 h, but exact viability values were not reported.

Coculturing on microfluidic devices can also take place in chambers connected using microgrooves. Such a device was used to observe the transfer of exosomes containing Tau proteins from neurons on the somal side of the grooves to neurons on the neuritic side.[71] Dendrites from each side that extended into the microgrooves were shown to facilitate exosome transfer. Another incarnation of a microfluidic coculture system used a permeable polycarbonate membrane to separate neurocytes (PC12) from nephrocytes (293 cells).[72] In this device, soluble factors from the differentiated PC12 cells were shown to diffuse through the membrane to stimulate the secretion of epinephrine from the 293 cells. The epinephrine was measured via a mass spectrometric analysis of the cellular media collected from the microchannels without pretreatment.

The coculturing of cells can also be achieved by simply creating two chambers and connecting them via microfluidic channels. This method is particularly useful if one would like to take the "modified" effluent from one culture to measure its effects on another cell type. One particularly interesting example of such a device used a coculture of human myocardial cells and cancerous hepatocytes to better understand the cytotoxic effects of doxorubicin and its metabolites on the cardiomyocytes.[73] In this device, a series of Quake-style soft lithographic valves and pumps were used to create and direct a recirculating flow between the two chambers. Other channels were used to load cells, cell matrix, and staining materials through the activation of valves in those channels.

The coculturing of bacteria can be achieved in single droplets. Recently, a microfluidic water in oil in water droplet scheme was reported to select nonpathogenic bacterial populations (effectors) that were capable of reducing the population of pathogenic bacteria.[74] In this experiment, the effectors were cocultured with GFP producing pathogenic bacteria in droplets. A series of fluorescent staining steps were used to identify whether the effector, pathogen, both, or neither were killed or grew while

DOI: 10.1021/acs.analchem.7b04519
Anal. Chem. 2018, 90, 65−85

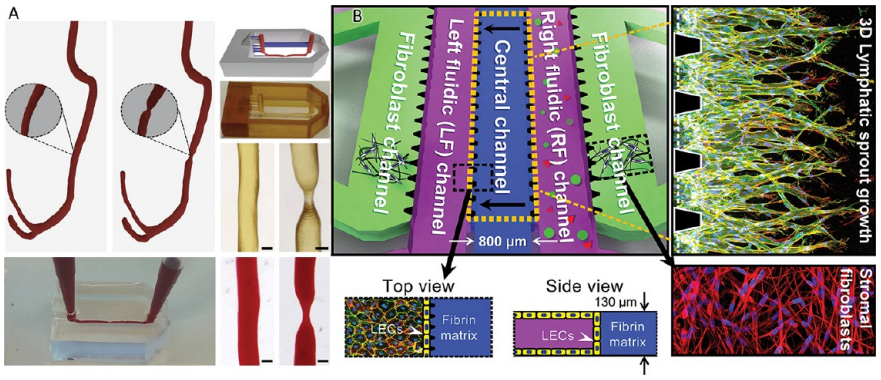

Figure 7. (A) Artificial PMDS blood vessel fabricated with 3D printed mold (left: healthy; right: diseased). Adapted from Costa, P. F.; Albers, H. J.; Linssen, J. E. A.; Middelkamp, H. H. T.; van der Hout, L.; Passier, R.; van den Berg, A.; Malda, J.; van der Meer, A. D. *Lab Chip* **2017**, *17*, 2785−2792 (ref 76). Published by The Royal Society of Chemistry. (B) Schematic overview of the device for three-dimensional coculture of lymphatic endothelial cells and stromal fibroblast cells. Reprinted from *Biomaterials*, *78*, S. Kim, M. Chung and N. L. Jeon, Three-dimensional biomimetic model to reconstitute sprouting lymphangiogenesis in vitro, 115−128, Copyright 2016, with permission from Elsevier (ref 77).

being cultured in the droplets. The droplets were sorted by FACS to isolate those effectors that optimally killed the pathogens or significantly reduced the growth rate of the pathogen. A large number of bacteria from a single strain could be analyzed for biodiversity with respect to their effects on pathogen growth.

The transition from simple cocultures to tissue-like systems is a continuum. One recently reported device that lies in the transition between the two seeks to mimic the T-cell zone in lymph nodes.[75] In this simple device, antigen bearing dendritic cells (DCs) were cultured and antigen specific T cells were flowed over them. Antigen specific and nonspecific attachment of CH4+ and CD8+ cells to the DCs was examined as a function of shear stress. Another transitional model included a microfluidic pillar array device to examine wound healing and the interplay between a 3D extracellular matrix and 3 cell types, keratocytes, dermal fibroblasts, and human umbilical vein endothelial cells. Results showed that cell attachment, morphology, cytoskeleton distribution, and nucleus shape were strongly influenced by the presence of the pillars. Cocultures of the 3 cell types on the pillar substrates indicated positive synergistic effects of the 3 cell types toward improving wound healing.

Analysis of Tissue and Organ Culture Models. The next step in advancing microfluidic-based cell culturing and chemical analysis beyond cocultures is the development of tissues and organs or organ systems to better help understand how such systems work, how disease processes progress, and how drugs are distributed and metabolized. Most of these systems need to be able to effectively generate 3D environments similar to their in vivo counterparts. Some outstanding papers in this area have been recently published which show that microfluidic devices are moving quickly to create near in vivo like conditions on chips.

One example of an in vitro system whose 3D shape is critical in order to replicate in vivo conditions as closely as possible is the vascular system. In a recent report, the 3D geometry of healthy and diseased arteries was replicated in a microfluidic device by 3D printing a mold with vessels on the order of 400 μm with feature sizes down to 25 μm (Figure 7A).[76] PDMS devices were created using these molds and seeded with human umbilical vein endothelial cells grown to confluence. Computational fluid dynamics was used to investigate the appropriate flow and shear rates to use in these devices when loaded with human whole blood. Thrombosis was seen in stenotic geometries but not healthy ones.

Other forms of vasculature found in the body are lymphatic vessels. In an attempt to replicate such an environment, a multichannel microfluidic device was fabricated to coculture stromal fibroblasts and lymphatic endothelial cells (LECs) (Figure 7B).[77] In the central channel, LECs were grown while on the outside channels fibroblasts were grown. The two channels on either side of the central channel were used to deliver biological factors or to allow flow-mediated stimulation. Experiments carried out on this device showed that soluble factors from stromal fibroblasts and interstitial flow significantly influenced lymphangiogenesis.

Microfluidic cell culturing devices can also be used to culture tumors. In a recent report, a cell culturing device using a microwell array assisted by ultrasonic standing waves was used to gently nucleate human hepatocellular carcinoma tumors.[78] The growth of these tumors was characterized using optical spectroscopy. Natural killer (NK) cells were then added at different tumor/NK cell ratios, and the behavior of the system was monitored. This approach is generic in nature and should be applicable to a wide variety of tumor and tissue culture model systems. It is, however, quite simple and does not mimic a normal tumor environment. In order to more accurately simulate the tumor microenvironment, a microfluidic culturing device was reported in which the necrotic, hypoxic, and normoxic core of a nonvascularized tumor was simulated in a microchamber using U-251 MG cells embedded in a collagen matrix that was situated between two perfusion channels that were 2 mm apart.[79] Glucose and oxygen levels, as well as cell death, were monitored spatially in the tumor using fluorescent probes. Drug toxicity assays were also performed. The authors claimed that the ability to culture the cells in a more relevant biological environment will lead to more realistic results in terms of the use of chemotherapy agents on tumors.

While the ability to create tumor models in vitro has advantages in terms of simplicity, the biological relevance of such an approach may ultimately limit what can be learned. The ability to culture microdissected tumor tissues on a microfluidic device might significantly increase the biological relevance as has been recently reported using a simple serpentine device.[80] This device had a series of depressions in the channel that could capture ∼400 μm diameter microdissected tumors for culturing. The capture and culture of eight different types of tumor tissues were demonstrated along with a chemosensitivity test that could significantly impact chemotherapy treatment success rates.

DOI: 10.1021/acs.analchem.7b04519
Anal. Chem. 2018, 90, 65−85

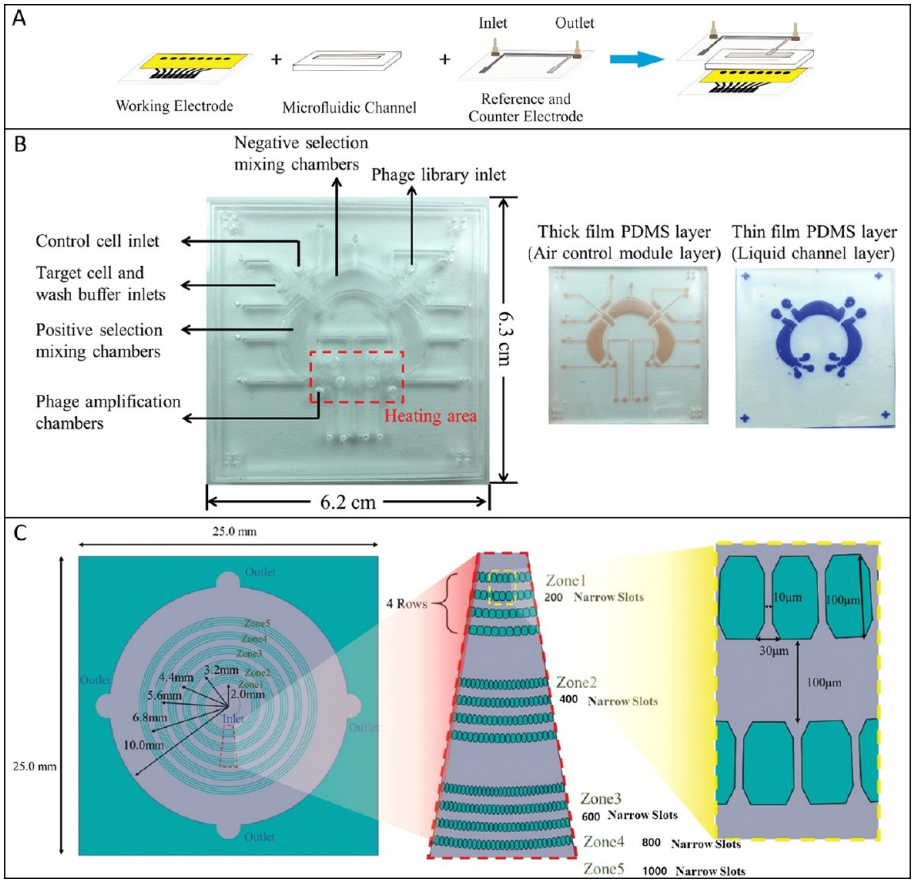

Figure 8. (A) Construction of disposable immunoassay device. Adapted from de Oliveira, R. A. G.; Materon, E. M.; Melendez, M. E.; Carvalho, A. L.; Faria, R. C. *ACS Applied Materials & Interfaces* **2017**, *9*, 27433−27440 (ref 88). Copyright 2017 American Chemical Society. (B) Microfluidic chip design for screening of phage-displayed peptides. Reprinted from Che, Y.-J.; Wu, H.-W.; Hung, L.-Y.; Liu, C.-A.; Chang, H.-Y.; Wang, K.; Lee, G.-B. *Biomicrofluidics* **2015**, *9*, 054121 (ref 89), with the permission of AIP Publishing. (C) Pillar-based device for gauging mechanical deformability of cells. Reprinted from *Sensors and Actuators, B: Chemical, 244*, J. Bu, T. H. Lee, I. S. Kim and Y.-H. Cho, Microfluidic-based mechanical phenotyping of cells for the validation of epithelial-to-mesenchymal-like transition caused by insufficient heat treatment, 591−598, Copyright 2017, with permission from Elsevier (ref 96).

One of the most sought after physiological models to recreate in vitro is the blood−brain barrier (BBB). This barrier prevents the flow of many pharmaceutical agents into the brain. A viable model of this neurovascular layer along with the addition of a variety of brain cells types would be helpful in testing the ability of compounds to make it through this barrier and to act on such cells. A simple model of this barrier was reported using a hydrophilized PTFE nanoporous membrane rather than the more commonly used polyester membranes.[81] This transparent membrane was used to separate endothelial cells and astrocytes in a 3D hydrogel extracellular matrix (ECM) and allowed imaging of the barrier. On the endothelial side, appropriate shear stresses were replicated for proper cell growth and function. A more developed model of the BBB has also been reported.[82] This chip used a track etched polycarbonate membrane to separate human brain derived microvascular endothelial cells from brain cells supported in a 3D ECM. In this device, in addition to astrocytes, pericytes and neuronal cells were included to better simulate the brain parenchyma. Like the previously described model, the endothelial cells were cultured under shear stress. In addition, the membrane functionality was validated using fluorescence probes and electrical resistance measurements. In another report, transendothelial electrical resistance (TEER) measurements in a culture of hCMEC/D3 cerebral endothelial cells were used to demonstrate tight cellular junctions.[83] This measurement used a four-electrode system to generate an isolated TEER measurement independent of channel properties thus removing large measurement variations due to non-biological variables. One particular advantage of this system is that the electrodes are in the chip wells and so do not hamper microscopic viewing of the cells.

Another barrier that is of interest to recreate is that of the placenta as it too tightly regulates the substances that can pass through it. Recently, a porous membrane supported coculture mimicking this barrier was reported.[84] The polycarbonate membrane supported trophoblasts on one side and villous endothelial cells on the other in a physiologically relevant geometry. Continuous flow through the system created conditions for optimal cell growth and the correct localization of transport proteins. Glucose transfer rates across the microengineered barrier were similar to those in ex vivo perfused human placenta.

Like the multicell type BBB chip discussed above,[82] a physiologically relevant liver model was developed in a microfluidic cell culturing chip. The liver cell model included hepatocytes, endothelial cells, Kupffer cells, and Stellate cells in what the authors called a sequentially layered, self-assembly liver model (SQL-SAL).[85] The stated goal was to produce the simplest physiologically relevant device that would be reproducible and robust for 28 days to conduct liver studies. This quite

DOI: 10.1021/acs.analchem.7b04519
Anal. Chem. 2018, 90, 65−85

sophisticated, self-assembled tissue mimic contained labeled sentinel cells to measure apoptosis and reactive oxygen species to monitor cell health in the tissue mimic. Drugs, drug metabolites, albumin urea, and lactate dehydrogenase were also measured in the chip efflux. The mimic was challenged with multiple, different drugs, and mechanisms of cytotoxicity were determined.

An additional in vitro tissue model that is highly desired is that of the heart. A recent article reported that topographical cues molded in soft gelatin could coax human induced pluripotent stem cell-derived cardiomyocytes to form laminar cardiac tissues that resembled the native architecture of the heart.[86] With this system and the use of a multielectrode array, tissue-level electrophysiological responses were measured from the cells in the device. How these cardiac field potentials were affected by the administration of three cardiac relevant drugs was measured.

■ ANALYSIS OF INTACT CELLS WITH NO CULTURING

In the above section, we focused on performing qualitative or quantitative chemical or physical measurements from, for the most part, static cells in culture in microfluidic devices. In this section and those that follow, we will review papers that focused mainly on cellular measurements made on cells not specifically cultured on microfluidic devices. These measurements may be on intact cells or analytes secreted from cells or from lysate from lysed cells. The measurements may be carried out using fluorescence, electrochemistry, or mass spectrometry.

Fluorescence-Based Sensing. One of the major competitors to microfluidics for the analysis of cells is flow cytometry. Using flow cytometry, tens of thousands of cells can be analyzed quickly. Microfluidics cannot match the analysis rates of flow cytometers, but it can potentially make a larger number of more varied measurements than flow cytometers with potentially better absolute quantitation of intracellular species. This potential for better absolute quantitation is due to the flexibility that microfluidics offers in terms of the fabrication of the channel manifold geometry and the ability to run both cells and fluid boluses through the same channels. These advantages were recently shown in a microfluidic device that used a constriction area in a channel manifold that was smaller than the diameter of a cell.[87] The constriction forced cells to occupy the entirety of the fluorescence detection domain. This allowed the fluorescent signals from cells loaded with fluorescent antibodies to be quantitated by comparing the signals to those obtained from standard solutions flushed through the constricted detection channel.

One of the most straightforward and common methods of analyzing cells is through affinity interactions on the surfaces of cells that might indicate a certain disease condition. The most common affinity assay is the immunoassay. Microfluidic devices provide a good platform for a low-cost approach to the development of such assays for disease detection. For example, a disposable microfluidic immunoassay device (DμID) was reported for the detection of breast cancer using the carbohydrate antigen 15-3 (CA15-3).[88] This device consisted of 8 channels fabricated from a double-sided adhesive card and was shown have a 1200× lower LOD than other immunosensors reported in the literature (Figure 8A). The results were compared to a well-established conventional method and showed high correlation. In another PDMS-based microfluidic device, essentially the opposite approach was taken. With this device, the authors panned a phage display library to find peptides that would bind with high affinity and specificity to cancer cell types (Figure 8B).[89] Both positive and negative controls were used. Phages were initially mixed with negative control cells coated with magnetic beads. Phages that did not bind were moved to a second chamber where they were exposed to cancer cells coated with magnetic beads. The unbound phages were washed and removed. The phages on the target cell were amplified in *E. coli*. Six rounds of panning selection were performed. This resulted in peptides with K_d values in the nanomolar range. These peptides were then synthesized and used to specifically capture the cells lines they were panned against. The positive and negative selection, washing, and amplification were all carried out in a single integrated device molded from PDMS with soft lithographic valves used to control fluid pumping.

An interesting alternative affinity assay to measure galectin expression on neuroblastoma (NB) cells was carried out in a simple microfluidic device.[90] Galectin is overexpressed in this cancer cell line compared to normal cells. NB and control cells were captured on β-galactose beads coated on the bottom of a microfluidic channel. A galactoside probe was used to detect galectin expression on the cells. NB and control cells could be distinguished, and cell heterogeneity could be studied making this a potential screening tool for NB.

Mechanical Deformation. In addition to studying basic cell physiology, microfluidic devices have shown to be excellent platforms for disease diagnosis. Given the fact that molecular signatures from diseased cells are often in very low abundance and hard to directly visualize by labeling a specific molecule of interest with a fluorescent probe, indirect proxies indicative of (correlated with) disease states can potentially be used for diagnosis. Some of the most popular indirect proxies used are the mechanical properties of cells. Changes in these properties can also be used to study a cell's response to external stimuli. The central reason for the interest in studying the mechanical properties of cells is that they are directly related to the cytoskeleton composition.[91] Stem and cancerous cells are expected to have different mechanical properties as they have different cytoskeletal compositions. Recently, a method to differentiate stem cells and osteosarcoma's from other primary leucocyte lineages was demonstrated using a technique called real-time deformability cytometry.[92] This approach used a high-speed camera and detection algorithm to measure cell shapes as cells passed through a channel constriction under shear stress on a microfluidic device. This same approach was also used to examine F-actin, microtubule, and nuclear chromatin structure changes in human leukemia cells as a function of drug administration.[91] Changes in F-actin and microtubule were correlated with deformability changes, but chromatin alterations were not. Changes in deformation with the administration of drugs whose mode of action was to modify F-actin and microtubules could be measured. Continuous analysis rates of up to 1000 cells/h were demonstrated. A sophisticated numerical model simulating the effects seen in real-time deformability cytometry was developed and resulted in new measurements that could be included to distinguish between cortex and bulk elasticity deformation effects.[93] Another similar method to measure the deformability of cells was reported where, instead of examining the deformability in a constricted channel, cell deformability was examined as a function of shape change when the cell collided with a wall at the T-channel junction in a microfluidic device. A high-speed camera and algorithm allowed unattended automated analysis rates of 450 cells/s. With this device, large stiffness changes in cells were found to occur in both breast cancer progression and epithelial mesenchymal transition.

DOI: 10.1021/acs.analchem.7b04519
Anal. Chem. 2018, 90, 65−85

Deformability cytometry was also demonstrated in a device with a large number of parallel channels with decreasing widths along their lengths.[94] These channels were coated with an anti-EpCAM antibody. The travel length of a cell through a channel was shown to be correlated with its size, deformability, and the expression of EpCAM on the cell surface. The pressure needed to push the cells through the channels was used as a proxy for a combination of these variables. Some cancer cell lines could be distinguished from noncancerous cells using this technique.

Another approach to measure cell size and deformability used a series of pillar regions with sequentially decreasing spacing.[95] U-251 cells were captured, and their resistance to vincristine was analyzed as a function of biomechanical properties. Small, deformable cells were more resistant than larger, stiffer cells. A different pillar-based device for measuring cell deformability used a series of 5 concentric rings of pillars with 10 μm spacing between the pillars in each ring (Figure 8C).[96] Cells were added in the center and pushed outward through the rings of pillars. The force applied to each subsequent ring was lower due to the larger number of pillars. The more deformable the cell, the farther outward it moved. This device was used to gauge the effectiveness of hyperthermic cancer treatment. The higher the temperature applied to the cells, the more deformable the cells were under nonlethal hyperthermia conditions. A much slower approach to performing cell deformability measurements was reported using a cross-slot flow microfluidic device.[97,98] In these devices, flow entered into a cross-intersection from two opposite arms and exited through the others creating a stagnation point in the center. Cells in the center were subjected to elongational viscous fluid stresses. In one report, 3T3 fibroblasts and tumor initiating cells were shown to change their elastic modulus when the cells were exposed to cytoskeleton softening or stiffening agents.[97] In the other report using a very similar setup, various types of stem cells and their derivatives were better characterized through a combination of sizing, morphology, deformation kinetics, and deformability properties obtained from the high-speed imaging of the cells.[98]

In a related vein, a very interesting device was reported to effectively measure the contractile force exhibited by platelets spanning 2 fibronectin microdots.[99] On this device, fibronectin microdots were attached to hydrogels of varying stiffness in several parallel microfluidic channels. Platelets added to the device and incubated under activating conditions would attach to a microdot, extend filipodia, and attach to the neighboring dot and contract. The change in microdot separation was used to measure the contractile force. Highly contractile subpopulations were found to be absent in patients with undiagnosed bleeding disorders. A different approach to measuring stretching involved situating a cell between two electrodes with an electric field applied across them to create a dielectrophoretic effect.[100] A low AC field was initially applied to attract a cell to one electrode via a p-DEP force. The voltage was then increased, and the change in cell size and shape was observed. The device was tested using Leukemia NB4 cells. When treated with all-trans retinoic acid, the measured cell deformation increased as expected.

Deformability is a measurement of cell shape changes under stress. Cell shape, in general, however, is itself a potential diagnostic, but in order to use it successfully in a high-throughput analysis regime, one needs to be able to perform rapid 3D imaging. There are several important diseases, for example, that affect the shape of red blood cells (RBCs). Recently, a 3D imaging technique was reported that is capable of performing complete morphological classification of RBCs without the need for mechanical or optoelectronic devices to control cell rotation.[101] By taking advantage of the random self-rotation of RBCs, RBCs were characterized on the basis of 3D morphology, corpuscular hemoglobin levels, volume, and refractive index. Anemic blood cells could be differentiated from normal RBCs in this device.[101] Another paper integrated imaging from a high-speed camera with impedance measurements to correlate physical morphologies with a cell's dielectric properties.[102] The cells were imaged while transiting through the impedance sensor in a microfluidic channel. The device could be trained via impedance signatures alone to differentiate between single and budding yeasts.

Analysis via Electrical Characteristics of Cells. The generic overall electrical properties of cells can also be used as a label-free method of differentiating cells. For example, isodielectric separation on a simple microfluidic device was used to differentiate between activated and nonactivated leukocytes.[103] This device consisted of electrodes patterned on two glass slides and separated by double stick tape to form a channel through which cells could be flowed. The ability to monitor sepsis progression in cecal ligation and punctive mice using human granulocytes was demonstrated. The results correlated well with flow cytometry assays under a wide variety of conditions.

Basic Biology Studies. There are a variety of advantages to using microfluidic devices for the study of basic biology that may or may not have relevance to diseases. The basic advantage of such devices is generally their ability to isolate individual organisms and track them through time under different environmental conditions. A great example of this is the use of a PDMS-based device consisting of a simple, single microfluidic channel interfaced with a glass coverslip to monitor irreversible and reversible adhesion events in single *Caulobactor crescentus* cells.[104] The fluorescently labeled cells were imaged as they flowed through a simple straight channel, and the adhesion events were detected at the glass surface. The interaction time between the glass surface and the cells determined whether the attachment was irreversible or not. This basic concept of monitoring cell attachment was expanded significantly in a second paper where the attachment and growth characteristics of dimorphic alphaproteobacterium cell types were examined.[105] The PDMS-based device with integrated soft lithographic valves allowed the culturing of a biofilm integrated with a downstream imaging area where cells released from the biofilm could attach and grow. The growth characteristics of these synchronized, motile cells were then characterized.

Growth dynamics from usually difficult to image biofilms can be obtained through the unique combination of microfluidic devices and NMR imaging.[106] The vacuum compatible device, SALVI (System for Analysis at the Liquid Vacuum Interface), was fabricated from PDMS, PTFE, PEEK, and SiN which did not generate proton signals. Only the fluid filled channels were imaged. Water diffusion, fluid velocities, and biofilm porosity were measured using the NMR imaging.

In addition to bacterial growth studies, the growth dynamics of viruses can also be studied. An elegant example of such a study made use of a glass microfluidic sensing device that was fabricated with a microchannel that incorporated 2 nanochannels in series to monitor the assembly of virus capsids.[107] These single-particle measurements took place under biologically relevant conditions using a resistive pulse sensing technique. With this technique, the electrical current through the micro−nano−micro channel system was monitored. As the virus capsids passed through a series of two nanochannels, the change in current flowing

DOI: 10.1021/acs.analchem.7b04519
Anal. Chem. 2018, 90, 65−85

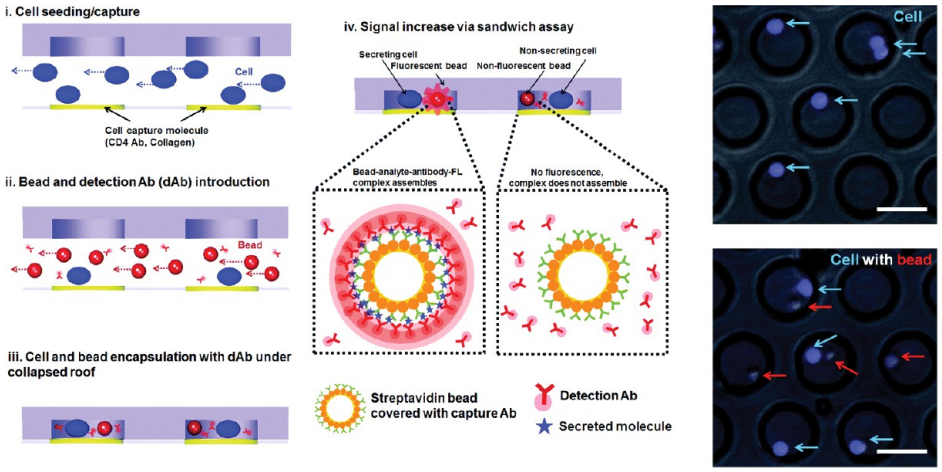

Figure 9. (left) Diagram of the reconfigurable microcompartment arrays for isolating single cells and sensing beads for monitoring cellular secretory activity. (right) Microscope image of cells and sensing beads encapsulated inside compartments. Adapted from Son, K. J.; Rahimian, A.; Shin, D.-S.; Siltanen, C.; Patel, T.; Revzin, A., *Analyst (Cambridge, United Kingdom)* **2016**, *141* (2), 679−688, (ref 114), with permission of The Royal Society of Chemistry.

through the system could be correlated with the type of capsid being assembled. This same device was also used to investigate how varying RNA length and poly(styrene) particle size affected particle assembly.[108] In this experiment, the current changed as the particles passed through the pores along with the transit time interval between the 2 nanopores. Size exclusion chromatography analysis of the particles collected from the chip indicated that the optimal substrate for the assembly of SV40 was determined by a complex interplay among capsid charge, capsid size, substrate length, and structure. An improved version of this device with 8 nanochannels in series was used to monitor the assembly of Hepatitis B capsids in real-time using both pulse amplitude and transit time between pores.[109] The standard deviations of the pulse amplitudes averaged across the 8 nanochannel constrictions decreased 2.7-fold compared to a single channel.

ANALYSIS OF SECRETED MOLECULES FROM INTACT CELLS

The ability to monitor and quantify biomolecules released into the extracellular environment is of particular interest to drug screening, drug discovery, diagnostics, and basic biology. The volume scale, channel manifold customizability, and potential for automation afforded by microfluidic devices provides a powerful platform from which to make short time scale resolved measurements of secreted signaling molecules from cells in response to perturbation. Discussed in the following section are several notable examples of advances enabled through the use of microfluidics in cell secretion studies.

Paper-based microfluidic devices have recently found their way into biological analyses due to their simplicity and cost-effectiveness. One noteworthy implementation of this technology featured dual photoelectrochemical (PEC) and colorimetric detection to monitor the release of H_2O_2 from MCF-7 cancer cells.[110] Cells were captured on the surface of vertically aligned bamboo-like ZnO structures grown on Pt nanoparticles on a working electrode. Decomposition of H_2O_2 was quantified on paper by measuring electron transfer from illuminated graphene quantum dots (GQDs) conjugated to DNA aptamers that were also attached to the working electrode. The sensitivity was improved by conjugating flower-like Au@Pd alloy nanoparticles to the aptamers to catalyze the formation of ·OH which cleaved the DNA strands allowing probes to migrate away from the working electrode, thus reducing the photocurrent signal. The released probes also catalyzed a chromogenic reaction with 3,3′,5,5′-tetramethylbenzidine (TMB), allowing the real-time visualization of H_2O_2 production. The inverse relationship between photocurrent and concentration of H_2O_2 led to an improvement in detection limits of approximately 5 orders of magnitude, with good linearity, over previously reported PEC techniques. The colorimetric detection method provided a modest improvement in detection limit over previous work, but the combination of simultaneous detection schemes can be used when low limits of detection are not required. These devices, while elegant, appear to require complex fabrication steps. Paper-based devices have also been used as a high surface area culture substrate for the analysis of anchorage dependent cells. One foray into this area involved the study of dopamine (DA) released from neuron-like PC12 cells upon exposure to the neurotransmitter acetylcholine.[111] The design used a PDMS/paper bioreactor connected to a downstream electrochemical detector (ECD). Cells in the bioreactor were exposed to acetylcholine which initiated the cascade that culminated in the release of DA that was swept downstream to the ECD. Good agreement between previous single cell studies and this known population of cells was achieved with respect to the amount of DA released, and a limit of detection of 4.6 ± 8.9 nM was achieved. The impact of L-3,4-dihydroxyphenylalanine (L-DOPA), a known DA release promoter, and dynasore, a drug reported to inhibit DA release, were also evaluated. Cheap, disposable, and yet quantitative devices for online monitoring of cellular responses will always find a welcome home with drug companies and researchers alike. The use of cheap materials and potentially reusable devices that can disassembled, cleaned, and reassembled with the paper substrate being the only consumable part is certainly an appealing option for large scale cellular testing of therapeutic agents like that which is necessary for screening libraries of active pharmaceutical ingredients (API).

Along those lines, other methods geared toward the analysis of organ-on-a-chip systems have been reported recently. For example, a bioinspired polymer gel sensor was used to image extracellular Ca^{2+}.[112] The polymer gel sensor was made of a

DOI: 10.1021/acs.analchem.7b04519
Anal. Chem. 2018, 90, 65−85

chemically cross-linked poly(acrylic acid) gel that aggregated in the presence of Ca^{2+}. Imaging of extracellular Ca^{2+} was enabled by attaching an aggregation-induced emission luminogen. The gel sensor showed good dynamic range and excellent selectivity toward Ca^{2+} over other biologically relevant ions. Another group reported a method that used a series of fluorogenic dyes designed to fluoresce in the presence of specific analytes or cellular conditions to study the profiles of oxygen and glucose concentrations inside the device and their effects on cell proliferation and growth, as well as ROS generation and apoptosis.[79] Real-time monitoring of glucose and ROS production in U-251 MG glioblastoma cells and HCT-116 colon cancer cells were achieved in a microfluidic device mimicking the extracellular matrix. Development of a realistic mimic of the tumor microenvironment as indicated with this device may help improve the effectiveness of chemotherapy and reduce the number of animals required for in vivo testing by serving as an intermediate between traditional cell culture and in vivo drug evaluation.

Immunofluorescence is another fluorescence-based detection method that has been applied to secreted molecule detection offering its own distinct advantages. One group combined surface plasmon resonance imaging (SPRi) and immunofluorescence to perform a long-term analysis in an integrated microfluidic device over the course of 24 h for immunofluorescence and up to 65 h for SPRi.[113] Interferon gamma (IFN-γ) and interleukin-2 (IL-2) levels from T-lymphocytes that were captured and cultured on a biochip were quantified using this dual-imaging detection method. Because the cells were captured using antibodies specific to cell type, this analysis enabled the monitoring of cytokines secreted by identified cells and may be further adapted to be compatible with various other cell types and other relevant cytokines. This system may also be further extended to enable the label-free and real-time measurement of multiple cytokines from individual cells. Another system has been developed to detect both IFN-γ from single $CD4^+$ cells and exosomes from HepG2 human hepatocellular carcinoma cells in a reconfigurable microfluidic device.[114] Cells were confined to ~7000 microcompartments (20 pL volume) along with sensing microbeads modified with capturing antibodies (Figure 9). The liquid inside the compartments contained fluorescently labeled secondary antibodies that bound to secreted molecules already bound to the capture antibodies causing the microbeads to become fluorescent. This approach could be adapted to monitor multiple cell-secreted signals and potentially combined with function-based single-cell sorting.

Enzyme-linked immunosorbent assays (ELISA) have gained popularity in the area of biomarker analysis due to their high sensitivity and selectivity. However, they have drawbacks in terms of time of analysis, required human intervention, and inability to provide semi-real time long-term monitoring. One solution to these challenges was the construction of a microfluidic device capable of continuous monitoring of biomarkers from human liver organoids.[115] Human serum albumin (HSA) and glutathione-*S*-transferase-alpha (GST-α) were captured by their respective antibodies which were secured to a gold working electrode (WE). The increased steric disruption upon antibody/antigen interaction resulted in an increase in the charge transfer resistance (R_{ct}) of the oxidation/reduction of ferrocyanide $[Fe(CN)_6^{3-/4-}]$ in the surrounding solution. One of the other unique features of this device is that, following a measurement, the WE could be stripped clean, refunctionalized with fresh antibodies, and prepared for a subsequent measurement in a fully automated fashion with negligible loss in electrode performance for up to 25 measurement cycles. This permitted the extended online study of cellular response to external stimuli, in this case acetaminophen, of a human liver organoid for up 7 days. The LODs for HSA and GST-α were 0.023 and 0.01 ng/mL, respectively. The ability to monitor cellular response to pharmaceutical candidate drugs online and over time is of ever growing importance in present day as drug companies are under increasing scrutiny to deliver effective and safe therapies. This biosensor exhibits marked improvement over traditional methods and also addresses some other aspects regarding pharmaceutical testing such as the ethics of animal testing and how truly representative animal responses are to candidate drugs designed for humans. One limitation of this biosensor is the need for an abundance of associated hardware including pumps, fluid reservoirs, computers, bioreactors, and WAGO controllers.

In addition to antibodies, aptamer-based detection schemes are also emerging as a method that offers comparable biomolecular specificity and greater stability compared to antibodies. Similar to some of the previously mentioned antibody-based methods, secretion of IFN-γ from single T-cells encapsulated in droplets was measured using a designed membrane-anchored fluorescent aptamer sensor.[116] The aptamer was anchored to the cell surface via hydrophobic interaction between the phospholipid layer and a cholesterol tail linked to the 5′end. The 5′ and 3′ ends of the aptamer were designed such that self-hybridization occurred yielding a hairpin structure. For fluorescence, the 5′ end was labeled with a ROX fluorophore and a TAO quencher was bound to the 3′ end. The loop portion of the aptamer would selectively bind IFN-γ, opening the hairpin structure and thus separating the fluorophore from the quencher to generate a fluorescence signal. High-throughput single-cell analyses such as this may significantly aid in the study of the heterogeneity of the immune response.

Like antibodies, aptamers may also be used in electrochemical-based detection of secreted molecules. An electrochemical impedimetric aptamer-based sensing device was developed to detect creatine kinase (CK)-MB secreted from cardiac organoids.[117] Using a surface bound aptamer sensor, changes in impedance from the binding of CK-MB released from embryonic stem cell-derived cardiomyocytes were monitored in a heart-on-a-chip system. The aptamers exhibited better stability and better sensitivity over the antibodies. Aptamers have the added advantage of maintaining their effectiveness over a wide range of temperature and pH where the function of the antibodies is limited to physiological conditions. The increased sensitivity of the aptamers was a product of reduced nonspecific binding versus their antibody counterparts. The limit of detection for CK-MB of the aptamer-based biosensor was 2.4 pg/mL.

While most of the secreted molecules discussed above were indirectly detected through conjugation with an affinity marker, direct detection through fluorescent derivatization is also possible. In one elegant example of this approach, 10 amino acids secreted by murine islets of Langerhans were derivatized using NDA and then separated via electrophoresis.[118] The device used for this analysis consisted of an integrated perfusion system for the islets, an islet chamber, a derivatization channel, a gated injection intersection, and a separation channel. Detection limits for the amino acids were in the low nM range, and secretion from the islets could be monitored for 2 h. The biological relevance was demonstrated by monitoring the change in amino acid

DOI: 10.1021/acs.analchem.7b04519
Anal. Chem. 2018, 90, 65−85

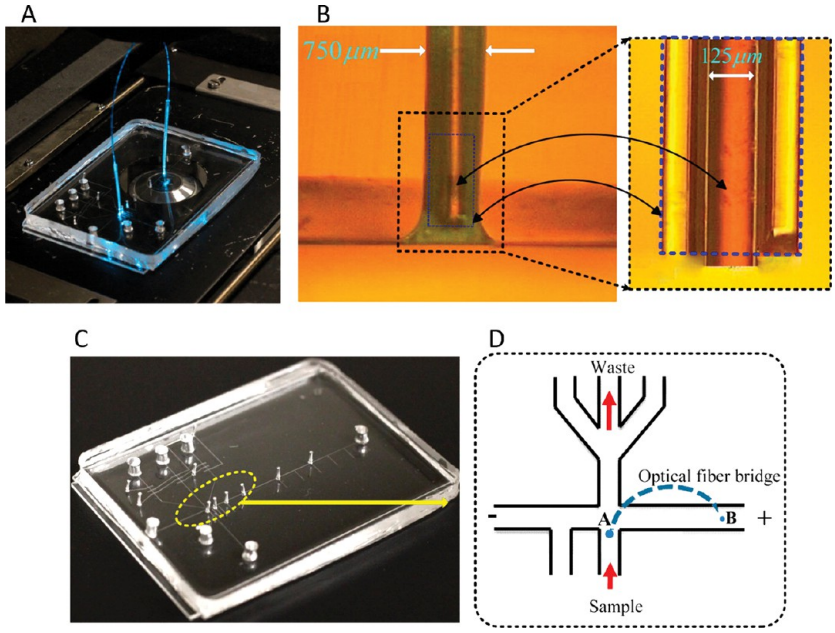

Figure 10. (A) Photograph of optical fiber bridge microfluidic device. (B) Close-up photograph of the optical fiber optic inserted through a plastic nozzle. (C and D) Photograph of the microfluidic device and expanded view of the cell lysing intersection. Adapted from Patabadige, D. E. W.; Sadeghi, J.; Kalubowilage, M.; Bossmann, S. H.; Culbertson, A. H.; Latifi, H.; Culbertson, C. T. *Analytical Chemistry* **2016**, *88*, 9920−9925 (ref 124). Copyright 2016 American Chemical Society.

concentrations as a function of changes in glucose concentration perfused over the cells. The ability to monitor changes in amino acid concentration in response to the addition of a known inhibitor of the proton motive force was also demonstrated. A similar device was modified to monitor insulin secretion from islet cells.[119] In this device, islet cells were again placed in a well and perfused with varying glucose concentrations via gravity fed flows. The effluent containing secreted insulin from the islet chamber was mixed with an insulin antibody and Cy5-labeled insulin to generate a competitive immunoassay. The fluorescence anisotropy of the Cy5-insulin was then measured. Temperature homogeneity and constant flow rate conditions were critical to the reproducibility of the assay. The limit of detection for the assay was 4 nM. In another approach to monitor insulin signaling, a 16-channel input/output multiplexer was developed.[120] This PDMS-based device allowed any combination of channels to collect effluent from or to send input to a central culture chamber that contained either islet cells or adipose tissue. The input/output configuration featured automated control using a series of soft-lithographic valves. To demonstrate the usefulness of the device, 90 min secretion profiles of ∼10 islet cells were measured. In addition to being able to quantitate cell secretion, cell responses to various inputs could also be monitored via imaging of the cell culture chamber. Fluorescent imaging of fatty acid uptake dynamics was measured in adipose tissue in response to insulin and glucose levels for 2.5 h.

■ ANALYSIS OF CELL LYSATES

One particular issue with analyzing intact cells is that the information density is low. One can only extract information for a few different parameters. This information is generally gained through staining with fluorescent dyes, and only a few dyes can be detected simultaneously due to spectral overlap. The analysis of intracellular analytes released through lysis followed by some separation method and detection increases substantially the number of analytes that can be simultaneously examined. This can provide a large amount of highly specific information regarding cellular heterogeneity. Presented below are recent advances in the lysis and analysis of single cell lysates.

The quantitation of multiple analytes can be a valuable tool in the study of single cells. One example that demonstrated multiplexed analysis in a microfluidic device was the analysis of four intracellular metal ions, Na^+, K^+, Ca^{2+}, and Mg^{2+}, in single PC-12 cells using multicolor fluorescence detection.[121] Metal ions were derivatized with fluorescent probes inside cells. Cells were then loaded onto the microfluidic device and lysed; the intracellular contents were electrophoretically separated, and the levels of intracellular metal ions were quantified. The results demonstrated that an imbalance in metal ions in neuron-like cells may have a synergistic function in the regulation of neurological diseases.

While laser-induced fluorescence is relatively popular in microfluidic devices as a mode of detection, there have been increased efforts toward integrating microfluidic devices with mass spectrometry (MS). Microfluidic MS systems are powerful tools for the sensitive and selective detection of intracellular molecules.[122] One such example is an automated microchip electrophoresis-mass spectrometric platform for the lysis and analysis of single cells.[123] Lysis was achieved by creating a cell-sized lysis zone where two nanoelectrodes were used to automatically lyse cells for electrophoretic separation and MS detection of intracellular analytes. The platform was used to determine intracellular levels of dopamine and glutamic acid in individual PC-12 neuronal cells.

A challenging topic associated with the automated lysis and analysis of single cells is balancing the hydrodynamic transport of cells with cell lysis and electrophoretic lysate injection into a separation channel. In an effort to address this issue, a device featuring integrated soft lithographic pumps to precisely control hydrodynamic pumping and cell transport on chip was reported.[124] With this device, the cell velocities through the lysis intersection and the injection of the lysate could be

DOI: 10.1021/acs.analchem.7b04519
Anal. Chem. 2018, 90, 65−85

controlled much more reproducibly than by using an external syringe pump to control fluid flow on the device. As a demonstration of throughput and stability, T-lymphocytes loaded with 2 fluorogenic dyes were analyzed at an average rate of 14 cells/min. The same group went on to improve upon their system by modifying the automated single cell analysis device to incorporate an optical fiber bridge that enabled fluorescence detection at multiple points of interest in the channel manifold.[125] This device required only one excitation source, one objective, and one detector (Figure 10). Using the optical fiber bridge, it was possible to determine when cells entered the separation channel for lysis, thus giving a start signal for the separation and enabling the determination of the absolute migration times of analytes. This newfound ability to determine absolute migration times allowed this method to be directly compared with traditional separation methods using traditional separation parameters such as plate number, plate height, and dispersion. A more sophisticated version of this device was reported in which light was focused into the multimodal fiber to generate a tunneling mode in the fiber.[126] This allowed the generation of 3 excitation and emission points using only one excitation source and detector. The light emanating from the fiber excited two points separated by ∼100 μm and allowed cell velocities to be measured as well as the injected lysate peak components.

In another approach to examining lysate from cells, an actively controlled water-in-oil droplet production system was combined with fluorescent detection using a lock-in amplifier to coordinate detection with droplet arrival at the detection point.[127] Droplets were alternately introduced into the oil stream from sample and reference side channels at a cross intersection. In this system, fatty acid uptake from lysed adipocytes was measured quantitatively. The adipocytes were cultured off chip, and lysates from single cells were introduced into the sample stream.

Single-cell DNA-based analysis has also taken advantage of the benefits offered by microfluidic technology. Single-cell 3′ mRNA counting was reported in a droplet-based system in which ∼250 000 single cells were analyzed across 29 samples.[128] 68 000 peripheral blood mononuclear cells were profiled using reverse transcription performed in the droplets. By using a computational method to analyze the data, donor cells could be distinguished from host cells in bone marrow transplant samples. Another droplet-based microfluidic platform used an RNA expression and protein sequencing assay to quantify proteins with 82 barcoded antibodies and >20 000 genes.[129] Cells were labeled with antibodies conjugated to DNA barcodes and then encapsulated in a droplet containing a gel-bead functionalized with an oligonucleotide containing identifying sequences as well as primers for PCR amplification. Using this approach, the effects of a CD27 agonist on human $CD8^+$ lymphocytes were assessed. Additionally, unknown outlier subpopulations, present among the enriched $CD8^+$ cells from 3 different donors, were identified, characterized, and found to share 17 differentially expressed proteins. Finally, DNA-based microfluidics has also been utilized to develop simplified instrumentation for detection of pathogens.[130] A functioning prototype of a lab-on-a-chip platform for the detection of pathogens using antibody-conjugated magnetic beads for pathogen isolation, followed by in-line DNA extraction, PCR amplification, and fluorescence detection, was presented. The prototype device, called the "MinoLyzer", accepted a custom-built microfluidic cartridge that could perform μL scale analyses on 1 mL samples. One of the more notable aspects of this cartridge is that it performed all of the required analysis steps without the integration of valves or actuators.

FUTURE OUTLOOK

The pace of advancement in cellular analysis capabilities on microfluidic devices continues to quicken. In this year's Review, more integrated devices than ever have been reported to culture and carry out sophisticated analyses on systems with multiple types of cells. The arrival of a variety of realistic in vitro liver and blood−brain barrier microfluidic devices for drug testing is just around the corner. The use of these devices in biotechnology to help select for high producing genetically modified organisms may also be expected to expand rapidly in the near future. This should also be true for devices to determine antibiotic resistance and for devices to identify new antibiotic sources. Another area of potential growth may revolve around the microbiome and the culturing/identification of new strains of bacteria. On the technological side, continued advances in 3D printing should assist in fabrication of increasingly complex channel manifolds with resolution approaching cellular dimensions. Finally, the increasing number of commercially available devices means that more of the analyses on these chips will become standard fare in biology, biochemistry, and medical laboratories. Further advances in the field will most likely come from integrated groups that consist of chemists, engineers, biologists, biochemists, and clinicians.

AUTHOR INFORMATION

Corresponding Author

*E-mail: culbert@ksu.edu. Phone: +1-785-532-6685. Fax: +1-785-532-6666.

ORCID

Christopher T. Culbertson: 0000-0002-6833-3237

Author Contributions

All authors contributed to the writing of the manuscript and have approved the final version.

Notes

The authors declare no competing financial interest.

Biographies

Jay Sibbitts received his B.S. degree in Chemistry from Truman State University in 2014. He is currently a graduate student in the Chemistry Department at Kansas State University. He is currently performing research in microfluidic single-cell analysis of signal transduction cascades.

Kathleen A. Sellens received her B.S. in Chemistry at McKendree University in 2012. Currently, she is a doctoral candidate in Analytical Chemistry at Kansas State University. She was a GK-12 (EIDRoP) NSF Fellow during the 2014−2015 school year and currently is working in the lab of Dr. Chris Culbertson focusing on the development of an isoelectric focusing microfluidic chip for enzyme activity monitoring via fluorescent peptide substrates.

Shu Jia received his B.S. degree in Chemistry from Sun Yat-sen University in 2014. He is currently a graduate student in the Chemistry Department at Kansas State University. His current work is focused on the automation of microfluidic isoelectric focusing devices with integrated sample preparation for enzyme activity assays.

Scott A. Klasner received his B.S. in Chemistry from Truman State University in 2003 and a Ph.D. in Chemistry from Kansas State University in 2010. He was most recently the Global Analytical Services Manager for Halliburton Energy Services based in Houston, TX where

DOI: 10.1021/acs.analchem.7b04519
Anal. Chem. 2018, 90, 65−85

he spent 7 years. He left that post in June 2017 due to complications resulting from ALS. He currently lives with his wife Sherry in the St. Louis, MO area.

Christopher T. Culbertson is a Professor of Chemistry at Kansas State University. He received a B.A. in Biology from Harvard in 1988, a B.S. in Chemistry from The University of West Florida in 1991, and a Ph.D. in Chemistry from the University of North Carolina at Chapel Hill in 1991. He was postdoctoral fellow at Oak Ridge National Laboratory from 1996 to 1997 and a staff member from 1997 to 2002. He has been at KSU since 2002.

■ ACKNOWLEDGMENTS

This research was funded by NSF Grant CHE-1411993 and CBET 1159966. S.J., K.A.S., and J.S. have been supported by the Terry Johnson Cancer Center, Kansas State University.

■ REFERENCES

(1) Culbertson, C. T.; Mickleburgh, T. G.; Stewart-James, S. A.; Sellens, K. A.; Pressnall, M. *Anal. Chem. (Washington, DC, U. S.)* **2014**, *86*, 95−118.
(2) Patabadige, D. E. W.; Jia, S.; Sibbitts, J.; Sadeghi, J.; Sellens, K.; Culbertson, C. T. *Anal. Chem. (Washington, DC, U. S.)* **2016**, *88*, 320−338.
(3) Roper, M. G. *Anal. Chem.* **2016**, *88*, 381−394.
(4) Akbari, S.; Pirbodaghi, T.; Kamm, R. D.; Hammond, P. T. *Lab Chip* **2017**, *17*, 2067−2075.
(5) Choi, C.-H.; Wang, H.; Lee, H.; Kim, J. H.; Zhang, L.; Mao, A.; Mooney, D. J.; Weitz, D. A. *Lab Chip* **2016**, *16*, 1549−1555.
(6) Chen, W.; Shu, Z.; Gao, D.; Shen, A. Q. *Adv. Healthcare Mater.* **2016**, *5*, 223−231.
(7) Cole, R. H.; Tang, S.-Y.; Siltanen, C. A.; Shahi, P.; Zhang, J. Q.; Poust, S.; Gartner, Z. J.; Abate, A. R. *Proc. Natl. Acad. Sci. U. S. A.* **2017**, *114*, 8728−8733.
(8) Jiang, C.-Y.; Dong, L.; Zhao, J.-K.; Hu, X.; Shen, C.; Qiao, Y.; Zhang, X.; Wang, Y.; Ismagilov, R. F.; Liu, S.-J.; Du, W. *Appl. Environ. Microbiol.* **2016**, *82*, 2210−2218.
(9) Nuti, N.; Verboket, P. E.; Dittrich, P. S. *Lab Chip* **2017**, *17*, 3112−3119.
(10) Tran, Q. D.; Kong, T. F.; Hu, D.; Marcos; Lam, R. H. W. *Lab Chip* **2016**, *16*, 2813−2819.
(11) Yeo, T.; Tan, S. J.; Lim, C. L.; Lau, D. P. X.; Chua, Y. W.; Krisna, S. S.; Iyer, G.; Tan, G. S.; Lim, T. K. H.; Tan, D. S. W.; Lim, W.-T.; Lim, C. T. *Sci. Rep.* **2016**, *6*, 22076.
(12) Chudziak, J.; Burt, D. J.; Mohan, S.; Rothwell, D. G.; Mesquita, B.; Antonello, J.; Dalby, S.; Ayub, M.; Priest, L.; Carter, L.; Krebs, M. G.; Blackhall, F.; Dive, C.; Brady, G. *Analyst (Cambridge, U. K.)* **2016**, *141*, 669−678.
(13) Dhar, M.; Karimi, A.; Che, J.; Rettig, M. B.; Di, C. D.; Wong, J.; Matsumoto, M.; Renier, C.; Sollier, E.; Triboulet, M.; Jeffrey, S. S.; Garon, E. B.; Goldman, J. W.; Kulkarni, R. P. *Biomicrofluidics* **2015**, *9*, 064116.
(14) Khojah, R.; Stoutamore, R.; Di Carlo, D. *Lab Chip* **2017**, *17*, 2542−2549.
(15) Wang, S.; Thomas, A.; Lee, E.; Yang, S.; Cheng, X.; Liu, Y. *Analyst (Cambridge, U. K.)* **2016**, *141*, 2228−2237.
(16) Paie, P.; Bragheri, F.; Di Carlo, D.; Osellame, R. *Microsystems & Nanoengineering* **2017**, *3*, 17027.
(17) Nam, J.; Tan, J. K. S.; Khoo, B. L.; Namgung, B.; Leo, H. L.; Lim, C. T.; Kim, S. *Biomicrofluidics* **2015**, *9*, 064117−064119.
(18) Zhao, J.; You, Z. *J. Micromech. Microeng.* **2015**, *25*, 125006−125012.
(19) Guo, F.; Mao, Z.; Chen, Y.; Xie, Z.; Lata, J. P.; Li, P.; Ren, L.; Liu, J.; Yang, J.; Dao, M.; Suresh, S.; Huang, T. J. *Proc. Natl. Acad. Sci. U. S. A.* **2016**, *113*, 1522−1527.
(20) Ma, Z.; Zhou, Y.; Collins, D. J.; Ai, Y. *Lab Chip* **2017**, *17*, 3176−3185.
(21) Yu, Z. T. F.; Joseph, J. G.; Liu, S. X.; Cheung, M. K.; Haffey, P. J.; Kurabayashi, K.; Fu, J. *Sens. Actuators, B* **2017**, *245*, 1050−1061.
(22) Yeo, J. C.; Lim, C. T.; Wang, Z. *Biomicrofluidics* **2015**, *9*, 054114.
(23) LaLonde, A.; Romero-Creel, M.; Saucedo-Espinosa, M.; Lapizco-Encinas, B. *Biomicrofluidics* **2015**, *9*, 064113.
(24) Chiu, T.-K.; Chou, W.-P.; Huang, S.-B.; Wang, H.-M.; Lin, Y.-C.; Hsieh, C.-H.; Wu, M.-H. *Sci. Rep.* **2016**, *6*, 32851.
(25) Khamenehfar, A.; Beischlag, T. V.; Russell, P. J.; Ling, M. T. P.; Nelson, C.; Li, P. C. H. *Biomicrofluidics* **2015**, *9*, 064104−064118.
(26) Madiyar, F. R.; Bhana, S.; Swisher, L. Z.; Culbertson, C. T.; Huang, X.; Li, J. *Nanoscale* **2015**, *7*, 3726−3736.
(27) Szydzik, C.; Khoshmanesh, K.; Mitchell, A.; Karnutsch, C. *Biomicrofluidics* **2015**, *9*, 064120.
(28) Lim, S. W.; Lance, S. T.; Stedman, K. M.; Abate, A. R. *J. Virol. Methods* **2017**, *242*, 14−21.
(29) Fiedler, B. L.; Van Buskirk, S.; Carter, K. P.; Qin, Y.; Carpenter, M. C.; Palmer, A. E.; Jimenez, R. *Anal. Chem. (Washington, DC, U. S.)* **2017**, *89*, 711−719.
(30) Sakuma, S.; Kasai, Y.; Hayakawa, T.; Arai, F. *Lab Chip* **2017**, *17*, 2760−2767.
(31) Xu, H.; Dong, B.; Xiao, Q.; Sun, X.; Zhang, X.; Lyu, J.; Yang, Y.; Xu, L.; Bai, X.; Zhang, S.; Song, H. *ACS Appl. Mater. Interfaces* **2017**, *9*, 30510−30518.
(32) Dey, S.; Vaidyanathan, R.; Carrascosa, L. G.; Shiddiky, M. J. A.; Trau, M. *ACS Sensors* **2016**, *1*, 399−405.
(33) Shi, W.; Wang, S.; Maarouf, A.; Uhl, C. G.; He, R.; Yunus, D.; Liu, Y. *Lab Chip* **2017**, *17*, 3291−3299.
(34) Green, B. J.; Kermanshah, L.; Labib, M.; Ahmed, S. U.; Silva, P. N.; Mahmoudian, L.; Chang, I. H.; Mohamadi, R. M.; Rocheleau, J. V.; Kelley, S. O. *ACS Appl. Mater. Interfaces* **2017**, *9*, 20435−20443.
(35) Li, W.; Zhang, Y.; Reynolds, C. P.; Pappas, D. *Anal. Chem. (Washington, DC, U. S.)* **2017**, *89*, 7340−7347.
(36) Marchalot, J.; Chateaux, J.-F.; Faivre, M.; Ferrigno, R.; Deman, A.-L.; Mertani, H. C. *Biomicrofluidics* **2015**, *9*, 054104.
(37) Fritzsch, F. S. O.; Blank, L. M.; Dusny, C.; Schmid, A. *Microfluid. Nanofluid.* **2017**, *21*, 1−10.
(38) Liu, C.; Guo, J.; Tian, F.; Yang, N.; Yan, F.; Ding, Y.; Wei, J. Y.; Hu, G.; Nie, G.; Sun, J. *ACS Nano* **2017**, *11*, 6968−6976.
(39) Zhang, P.; He, M.; Zeng, Y. *Lab Chip* **2016**, *16*, 3033−3042.
(40) Wang, J.; Li, W.; Zhang, L.; Ban, L.; Chen, P.; Du, W.; Feng, X.; Liu, B.-F. *ACS Appl. Mater. Interfaces* **2017**, *9*, 27441−27452.
(41) Fang, S.; Tian, H.; Li, X.; Jin, D.; Li, X.; Kong, J.; Yang, C.; Yang, X.; Lu, Y.; Luo, Y.; Lin, B.; Niu, W.; Liu, T. *PLoS One* **2017**, *12*, e0175050−e0175013.
(42) Zhao, Z.; Yang, Y.; Zeng, Y.; He, M. *Lab Chip* **2016**, *16*, 489−496.
(43) Wu, M.; Wang, Z.; Huang, P.-H.; Chen, C.; Huang, T. J.; Zhang, R.; Ouyang, Y.; Li, H.; Li, P.; Quinn, D.; Dao, M.; Suresh, S.; Sadovsky, Y. *Proc. Natl. Acad. Sci. U. S. A.* **2017**, *114*, 10584−10589.
(44) Subramanian, S.; Tolstaya, E. I.; Winkler, T. E.; Bentley, W. E.; Ghodssi, R. *ACS Appl. Mater. Interfaces* **2017**, *9*, 31362−31371.
(45) Rothbauer, M.; Praisler, I.; Ertl, P.; Docter, D.; Stauber, R. H. *Biosensors* **2015**, *5*, 736−749.
(46) Bonk, S. M.; Stubbe, M.; Tautorat, C.; Baumann, W.; Gimsa, J.; Buehler, S. M.; Klinkenberg, E.-D. *Biosensors* **2015**, *5*, 513−536.
(47) Boyce, M. W.; Kenney, R. M.; Truong, A. S.; Lockett, M. R. *Anal. Bioanal. Chem.* **2016**, *408*, 2985−2992.
(48) Kraemer, C. E. M.; Wiechert, W.; Kohlheyer, D. *Sci. Rep.* **2016**, *6*, 32104.
(49) Grünberger, A.; Probst, C.; Helfrich, S.; Nanda, A.; Stute, B.; Wiechert, W.; Von Lieres, E.; Nöh, K.; Frunzke, J.; Kohlheyer, D. *Cytometry, Part A* **2015**, *87*, 1101−1115.
(50) Kilinc, D.; Schwab, J.; Rampini, S.; Ikpekha, O. W.; Thampi, A.; Blasiak, A.; Li, P.; Schwamborn, R.; Kolch, W.; Matallanas, D.; Lee, G. U. *Integrative biology: quantitative biosciences from nano to macro* **2016**, *8*, 39−49.
(51) Uzel, S. G. M.; Amadi, O. C.; Pearl, T. M.; Lee, R. T.; So, P. T. C.; Kamm, R. D. *Small* **2016**, *12*, 612−622.
(52) Islam, T.; Resat, H. *Mol. BioSyst.* **2017**, *13*, 2069−2082.

DOI: 10.1021/acs.analchem.7b04519
Anal. Chem. 2018, 90, 65−85

(53) Martin, W. E.; Ge, N.; Srijanto, B. R.; Furnish, E.; Collier, C. P.; Trinkle, C. A.; Richards, C. I. *ACS Omega* **2017**, *2*, 3858−3867.
(54) Naskar, S.; Kumaran, V.; Basu, B. *ACS Biomater. Sci. Eng.* **2017**, *3*, 1154−1171.
(55) Shirani, E.; Razmjou, A.; Tavassoli, H.; Landarani-Isfahani, A.; Rezaei, S.; Abbasi Kajani, A.; Asadnia, M.; Hou, J.; Ebrahimi Warkiani, M. *Langmuir* **2017**, *33*, 5565−5576.
(56) Birchler, A.; Berger, M.; Jaggin, V.; Lopes, T.; Etzrodt, M.; Misun, P. M.; Pena-Francesch, M.; Schroeder, T.; Hierlemann, A.; Frey, O. *Anal. Chem. (Washington, DC, U. S.)* **2016**, *88*, 1222−1229.
(57) Wu, Y.; Gao, Q.; Nie, J.; Fu, J.-z.; He, Y. *ACS Biomater. Sci. Eng.* **2017**, *3*, 601−607.
(58) Cheng, Y.-H.; Chen, Y.-C.; Brien, R.; Yoon, E. *Lab Chip* **2016**, *16*, 3708−3717.
(59) Jin, S. H.; Lee, S. S.; Lee, B.; Jeong, S.-G.; Peter, M.; Lee, C.-S. *Anal. Chem.* **2017**, *89*, 9722−9729.
(60) Siedler, S.; Khatri, N. K.; Zsohar, A.; Kjaerboelling, I.; Vogt, M.; Hammar, P.; Nielsen, C. F.; Marienhagen, J.; Sommer, M. O. A.; Joensson, H. N. *ACS Synth. Biol.* **2017**, *6*, 1860−1869.
(61) Krone, K. M.; Warias, R.; Ritter, C.; Li, A.; Acevedo-Rocha, C.; Reetz, M. T.; Belder, D. *J. Am. Chem. Soc.* **2016**, *138*, 2102−2105.
(62) Junkin, M.; Kaestli, A. J.; Cheng, Z.; Jordi, C.; Albayrak, C.; Hoffmann, A.; Tay, S. *Cell Rep.* **2016**, *15*, 411−422.
(63) Vacchelli, E.; Ma, Y.; Baracco, E. E.; Sistigu, A.; Enot, D. P.; Pietrocola, F.; Yang, H.; Adjemian, S.; Chaba, K.; Semeraro, M.; Signore, M.; De Ninno, A.; Lucarini, V.; Peschiaroli, F.; Businaro, L.; Gerardino, A.; Manic, G.; Ulas, T.; Guenther, P.; Schultze, J. L.; et al. *Science (Washington, DC, U. S.)* **2015**, *350*, 972−978.
(64) Yuan, X.; Couto, J. M.; Glidle, A.; Song, Y.; Sloan, W.; Yin, H. *ACS Synth. Biol.* **2017**, in press; DOI: 10.1021/acssynbio.7b00177
(65) Yu, F. B.; Horowitz, M.; Willis, L.; Chau, R. M. W.; Zambon, A.; Bhaya, D.; Huang, K. C.; Quake, S. R. *BMC Biol.* **2017**, *15*, 11.
(66) Baltekin, O.; Boucharin, A.; Tano, E.; Andersson, D. I.; Elf, J. *Proc. Natl. Acad. Sci. U. S. A.* **2017**, *114*, 9170−9175.
(67) Baker, J. D.; Kysela, D. T.; Zhou, J.; Madren, S. M.; Wilkens, A. S.; Brun, Y. V.; Jacobson, S. C. *Anal. Chem. (Washington, DC, U. S.)* **2016**, *88*, 8476−8483.
(68) Nakaoka, H.; Wakamoto, Y. *PLoS Biol.* **2017**, *15*, e2001109.
(69) Yamada, A.; Renault, R.; Chikina, A.; Venzac, B.; Pereiro, I.; Coscoy, S.; Verhulsel, M.; Parrini, M. C.; Villard, C.; Viovy, J.-L.; Descroix, S. *Lab Chip* **2016**, *16*, 4691−4701.
(70) Sato, K.; Kikuchi, S.; Yoshida, E.; Ishii, R.; Sasaki, N.; Tsunoda, K.-i.; Sato, K. *Anal. Sci.* **2016**, *32*, 113−116.
(71) Wang, Y.; Balaji, V.; Kaniyappan, S.; Kruger, L.; Tepper, K.; Chandupatla, R.; Schneider, A.; Mandelkow, E.; Mandelkow, E.-M.; Irsen, S.; Maetzler, W. *Mol. Neurodegener.* **2017**, *12*, 5.
(72) Zhuang, Q.; Wang, S.; Zhang, J.; He, Z.; Li, H.; Ma, Y.; Lin, J.-M. *Sci. China: Chem.* **2016**, *59*, 243−250.
(73) Kamei, K.-i.; Kato, Y.; Hirai, Y.; Ito, S.; Satoh, J.; Oka, A.; Tsuchiya, T.; Chen, Y.; Tabata, O. *RSC Adv.* **2017**, *7*, 36777−36786.
(74) Terekhov, S. S.; Smirnov, I. V.; Stepanova, A. V.; Bobik, T. V.; Mokrushina, Y. A.; Ponomarenko, N. A.; Belogurov, A. A., Jr.; Rubtsova, M. P.; Kartseva, O. V.; Gomzikova, M. O.; Moskovtsev, A. A.; Bukatin, A. S.; Dubina, M. V.; Kostryukova, E. S.; Babenko, V. V.; Vakhitova, M. T.; Manolov, A. I.; Malakhova, M. V.; Kornienko, M. A.; Tyakht, A. V.; et al. *Proc. Natl. Acad. Sci. U. S. A.* **2017**, *114*, 2550−2555.
(75) Moura Rosa, P.; Gopalakrishnan, N.; Ibrahim, H.; Haug, M.; Halaas, Ø. *Lab Chip* **2016**, *16*, 3728−3740.
(76) Costa, P. F.; Albers, H. J.; Linssen, J. E. A.; Middelkamp, H. H. T.; van der Hout, L.; Passier, R.; van den Berg, A.; Malda, J.; van der Meer, A. D. *Lab Chip* **2017**, *17*, 2785−2792.
(77) Kim, S.; Chung, M.; Jeon, N. L. *Biomaterials* **2016**, *78*, 115−128.
(78) Christakou, A. E.; Ohlin, M.; Oenfelt, B.; Wiklund, M. *Lab Chip* **2015**, *15*, 3222−3231.
(79) Ayuso, J. M.; Virumbrales-Munoz, M.; Lacueva, A.; Lanuza, P. M.; Checa-Chavarria, E.; Botella, P.; Fernandez, E.; Doblare, M.; Allison, S. J.; Phillips, R. M.; Pardo, J.; Fernandez, L. J.; Ochoa, I. *Sci. Rep.* **2016**, *6*, 36086.
(80) Astolfi, M.; Peant, B.; Lateef, M. A.; Rousset, N.; Kendall-Dupont, J.; Carmona, E.; Monet, F.; Saad, F.; Provencher, D.; Mes-Masson, A.; Gervais, T. *Lab Chip* **2016**, *16*, 312−325.
(81) Sellgren, K. L.; Hawkins, B. T.; Grego, S. *Biomicrofluidics* **2015**, *9*, 061102.
(82) Brown, J. A.; Pensabene, V.; Markov, D. A.; Allwardt, V.; Neely, M. D.; Shi, M.; Britt, C. M.; Hoilett, O. S.; Yang, Q.; Brewer, B. M.; Samson, P. C.; McCawley, L. J.; May, J. M.; Webb, D. J.; Li, D.; Bowman, A. B.; Reiserer, R. S.; Wikswo, J. P. *Biomicrofluidics* **2015**, *9*, 054124.
(83) van der Helm, M. W.; Odijk, M.; Frimat, J.-P.; van der Meer, A. D.; Eijkel, J. C. T.; van den Berg, A.; Segerink, L. I. *Biosens. Bioelectron.* **2016**, *85*, 924−929.
(84) Blundell, C.; Tess, E. R.; Schanzer, A. S. R.; Coutifaris, C.; Su, E. J.; Parry, S.; Huh, D. *Lab Chip* **2016**, *16*, 3065−3073.
(85) Vernetti, L. A.; Senutovitch, N.; Boltz, R.; DeBiasio, R.; Ying Shun, T.; Gough, A.; Taylor, D. L. *Exp. Biol. Med.* **2016**, *241*, 101−114.
(86) Kujala, V. J.; Pasqualini, F. S.; Goss, J. A.; Nawroth, J. C.; Parker, K. K. *J. Mater. Chem. B* **2016**, *4*, 3534−3543.
(87) Li, X.; Fan, B.; Cao, S.; Chen, D.; Zhao, X.; Men, D.; Yue, W.; Wang, J.; Chen, J. *Lab Chip* **2017**, *17*, 3129−3137.
(88) de Oliveira, R. A. G.; Materon, E. M.; Melendez, M. E.; Carvalho, A. L.; Faria, R. C. *ACS Appl. Mater. Interfaces* **2017**, *9*, 27433−27440.
(89) Che, Y.-J.; Wu, H.-W.; Hung, L.-Y.; Liu, C.-A.; Chang, H.-Y.; Wang, K.; Lee, G.-B. *Biomicrofluidics* **2015**, *9*, 054121.
(90) Pastorino, F.; Ponzoni, M.; Simone, G. *Proteomics: Clin. Appl.* **2017**, *11*, 1600116.
(91) Golfier, S.; Rosendahl, P.; Mietke, A.; Herbig, M.; Guck, J.; Otto, O. *Cytoskeleton* **2017**, *74*, 283−296.
(92) Xavier, M.; Rosendahl, P.; Herbig, M.; Krater, M.; Spencer, D.; Bornhauser, M.; Oreffo, R. O. C.; Morgan, H.; Guck, J.; Otto, O. *Integrative Biology* **2016**, *8*, 616−623.
(93) Mokbel, M.; Mokbel, D.; Mietke, A.; Traeber, N.; Girardo, S.; Otto, O.; Guck, J.; Aland, S. *ACS Biomater. Sci. Eng.* **2017**, *3*, 2962−2973.
(94) Hu, S.; Liu, G.; Chen, W.; Li, X.; Lu, W.; Lam, R. H. W.; Fu, J. *Small* **2016**, *12*, 2300−2311.
(95) Pang, L.; Liu, W.; Tian, C.; Xu, J.; Li, T.; Chen, S.-W.; Wang, J. *Lab Chip* **2016**, *16*, 4612−4620.
(96) Bu, J.; Lee, T. H.; Kim, I. S.; Cho, Y.-H. *Sens. Actuators, B* **2017**, *244*, 591−598.
(97) Guillou, L.; Dahl, J. B.; Lin, J.-M. G.; Barakat, A. I.; Husson, J.; Muller, S. J.; Kumar, S. *Biophys. J.* **2016**, *111*, 2039−2050.
(98) Lin, J.; Kim, D.; Tse, H. T.; Tseng, P.; Peng, L.; Dhar, M.; Karumbayaram, S.; Di Carlo, D. *Microsystems & Nanoengineering* **2017**, *3*, 17013.
(99) Myers, D. R.; Qiu, Y.; Fay, M. E.; Tennenbaum, M.; Chester, D.; Cuadrado, J.; Sakurai, Y.; Baek, J.; Tran, R.; Ciciliano, J. C.; Ahn, B.; Mannino, R. G.; Bunting, S. T.; Bennett, C.; Briones, M.; Fernandez-Nieves, A.; Smith, M. L.; Brown, A. C.; Sulchek, T.; Lam, W. A. *Nat. Mater.* **2017**, *16*, 230−235.
(100) Zhang, X.; Chu, H. K.; Zhang, Y.; Bai, G.; Wang, K.; Tan, Q.; Sun, D. *J. Micromech. Microeng.* **2015**, *25*, 105004−105010.
(101) Merola, F.; Memmolo, P.; Miccio, L.; Savoia, R.; Mugnano, M.; Fontana, A.; D'Ippolito, G.; Sardo, A.; Iolascon, A.; Gambale, A.; Ferraro, P. *Light: Sci. Appl.* **2017**, *6*, e16241.
(102) Haandbaek, N.; Burgel, S. C.; Rudolf, F.; Heer, F.; Hierlemann, A. *ACS Sensors* **2016**, *1*, 1020−1027.
(103) Prieto, J. L.; Su, H.-W.; Hou, H. W.; Vera, M. P.; Levy, B. D.; Baron, R. M.; Han, J.; Voldman, J. *Lab Chip* **2016**, *16*, 4333−4340.
(104) Hoffman, M. D.; Zucker, L. I.; Brown, P. J. B.; Kysela, D. T.; Brun, Y. V.; Jacobson, S. C. *Anal. Chem. (Washington, DC, U. S.)* **2015**, *87*, 12032−12039.
(105) Williams, M.; Hoffman, M. D.; Daniel, J. J.; Madren, S. M.; Dhroso, A.; Korkin, D.; Givan, S. A.; Jacobson, S. C.; Brown, P. J. B. *J. Bacteriol.* **2016**, *198*, 1149−1159.
(106) Renslow, R. S.; Marshall, M. J.; Tucker, A. E.; Chrisler, W. B.; Yu, X. Y. *Analyst (Cambridge, U. K.)* **2017**, *142*, 2363−2371.
(107) Harms, Z. D.; Selzer, L.; Zlotnick, A.; Jacobson, S. C. *ACS Nano* **2015**, *9*, 9087−9096.

DOI: 10.1021/acs.analchem.7b04519
Anal. Chem. 2018, 90, 65−85

(108) Li, C.; Kneller, A. R.; Jacobson, S. C.; Zlotnick, A. *ACS Chem. Biol.* **2017**, *12*, 1327−1334.
(109) Kondylis, P.; Zhou, J.; Harms, Z. D.; Kneller, A. R.; Lee, L. S.; Zlotnick, A.; Jacobson, S. C. *Anal. Chem. (Washington, DC, U. S.)* **2017**, *89*, 4855−4862.
(110) Li, L.; Zhang, Y.; Zhang, L.; Ge, S.; Liu, H.; Ren, N.; Yan, M.; Yu, J. *Anal. Chem. (Washington, DC, U. S.)* **2016**, *88*, 5369−5377.
(111) Trouillon, R.; Gijs, M. A. M. *RSC Adv.* **2016**, *6*, 31069−31073.
(112) Ishiwari, F.; Hasebe, H.; Matsumura, S.; Hajjaj, F.; Horii-Hayashi, N.; Nishi, M.; Someya, T.; Fukushima, T. *Sci. Rep.* **2016**, *6*, 24275.
(113) Baganizi, D. R.; Leroy, L.; Laplatine, L.; Fairley, S. J.; Heidmann, S.; Menad, S.; Livache, T.; Marche, P.; Roupioz, Y.; et al. *Biosensors* **2015**, *5*, 750−767.
(114) Son, K. J.; Rahimian, A.; Shin, D.-S.; Siltanen, C.; Patel, T.; Revzin, A. *Analyst (Cambridge, U. K.)* **2016**, *141*, 679−688.
(115) Shin, S. R.; Kilic, T.; Zhang, Y. S.; Avci, H.; Hu, N.; Kim, D.; Branco, C.; Aleman, J.; Massa, S.; Silvestri, A.; Kang, J.; Desalvo, A.; Abdullah Hussaini, M.; Chae, S.-K.; Polini, A.; Bhise, N.; Hussain, M. A.; Lee, H. Y.; Dokmeci, M. R.; Khademhosseini, A. *Advanced Science (Weinheim, Germany)* **2017**, *4*, n/a.
(116) Qiu, L.; Wimmers, F.; Weiden, J.; Heus, H. A.; Tel, J.; Figdor, C. G. *Chem. Commun. (Cambridge, U. K.)* **2017**, *53*, 8066−8069.
(117) Shin, S. R.; Zhang, Y. S.; Kim, D.-J.; Manbohi, A.; Avci, H.; Silvestri, A.; Aleman, J.; Hu, N.; Kilic, T.; Keung, W.; Righi, M.; Assawes, P.; Alhadrami, H. A.; Li, R. A.; Dokmeci, M. R.; Khademhosseini, A. *Anal. Chem. (Washington, DC, U. S.)* **2016**, *88*, 10019−10027.
(118) Wang, X.; Yi, L.; Roper, M. G. *Anal. Chem. (Washington, DC, U. S.)* **2016**, *88*, 3369−3375.
(119) Schrell, A. M.; Mukhitov, N.; Yi, L.; Adablah, J. E.; Menezes, J.; Roper, M. G. *Anal. Methods* **2017**, *9*, 38−45.
(120) Li, X.; Brooks, J. C.; Hu, J.; Ford, K. I.; Easley, C. J. *Lab Chip* **2017**, *17*, 341−349.
(121) Li, L.; Fan, Y.; Li, Q.; Sheng, R.; Si, H.; Fang, J.; Tong, L.; Tang, B. *Anal. Chem. (Washington, DC, U. S.)* **2017**, *89*, 4559−4565.
(122) Jie, M.; Mao, S.; Li, H.; Lin, J.-M. *Chin. Chem. Lett.* **2017**, *28*, 1625−1630.
(123) Li, X.; Zhao, S.; Hu, H.; Liu, Y.-M. *Journal of Chromatography A* **2016**, *1451*, 156−163.
(124) Patabadige, D. E. W.; Mickleburgh, T.; Ferris, L.; Brummer, G.; Culbertson, A. H.; Culbertson, C. T. *Electrophoresis* **2016**, *37*, 1337−1344.
(125) Patabadige, D. E. W.; Sadeghi, J.; Kalubowilage, M.; Bossmann, S. H.; Culbertson, A. H.; Latifi, H.; Culbertson, C. T. *Anal. Chem. (Washington, DC, U. S.)* **2016**, *88*, 9920−9925.
(126) Sadeghi, J.; Patabadige, D. E. W.; Culbertson, A. H.; Latifi, H.; Culbertson, C. T. *Lab Chip* **2017**, *17*, 145−155.
(127) Negou, J. T.; Avila, L. A.; Li, X.; Hagos, T. M.; Easley, C. J. *Anal. Chem. (Washington, DC, U. S.)* **2017**, *89*, 6153−6159.
(128) Zheng, G. X. Y.; Terry, J. M.; Belgrader, P.; Ryvkin, P.; Bent, Z. W.; Wilson, R.; Ziraldo, S. B.; Wheeler, T. D.; McDermott, G. P.; Zhu, J.; Gregory, M. T.; Shuga, J.; Montesclaros, L.; Underwood, J. G.; Masquelier, D. A.; Nishimura, S. Y.; Schnall-Levin, M.; Wyatt, P. W.; Hindson, C. M.; Bharadwaj, R.; et al. *Nat. Commun.* **2017**, *8*, 14049.
(129) Peterson, V. M.; Zhang, K. X.; Kumar, N.; Wong, J.; Li, L.; Wilson, D. C.; Moore, R.; McClanahan, T. K.; Sadekova, S.; Klappenbach, J. A. *Nat. Biotechnol.* **2017**, *35*, 936−939.
(130) Sandetskaya, N.; Moos, D.; Poetter, H.; Seifert, S.; Jenerowicz, M.; Becker, H.; Zilch, C.; Kuhlmeier, D. *Future Science OA* **2017**, *3*, FSO177.

DOI: 10.1021/acs.analchem.7b04519
Anal. Chem. 2018, 90, 65−85